FEDERAL UNIVERSITY OF SÃO CARLOS
CENTER FOR HARD SCIENCES AND TECHNOLOGY
GRADUATE PROGRAM IN MATERIALS SCIENCE AND ENGINEERING

PRODUCTION AND MICROSTRUCTURE-PROPERTY CORRELATIONS IN MONO-ORIENTED BACTERIAL CELLULOSE MEMBRANES

Anderson Zhong Fan

São Carlos-SP
2024

FEDERAL UNIVERSITY OF SÃO CARLOS
CENTER FOR HARD SCIENCES AND TECHNOLOGY
GRADUATE PROGRAM IN MATERIALS SCIENCE AND ENGINEERING

PRODUCTION AND MICROSTRUCTURE-PROPERTY CORRELATIONS IN MONO-ORIENTED BACTERIAL CELLULOSE MEMBRANES

Anderson Zhong Fan

MSc Dissertation presented to the Graduate Program in Materials Science and Engineering as a partial requirement for the MASTER'S DEGREE IN MATERIALS SCIENCE AND ENGINEERING.

Advisor: Dr. Luiz Henrique Capparelli Mattoso
Co-advisor: Dr. Caio Gomide Otoni
Funding Agency: CAPES (Process: 88887.671697/2022-00)

São Carlos-SP
2024

DEDICATION

I dedicate this work to my parents and all my family and friends, for having placed all their trust in my future, and for enduring and supporting me in my moments of frustration. Especially to my father Nian (*in-memoriam*) who always supported me in my dreams and showed a great example of effort and dedication, and my best friend and girlfriend Luciana, for her presence and unconditional support.

CANDIDATE'S VITAE

Bachelor of Materials Engineering from the Federal University of Cariri (2020)

UNIVERSIDADE FEDERAL DE SÃO CARLOS

Centro de Ciências Exatas e de Tecnologia
Programa de Pós-Graduação em Ciência e Engenharia de Materiais

Folha de Aprovação

Defesa de Dissertação de Mestrado do candidato Anderson Zhong Fan, realizada em 07/03/2024.

Comissão Julgadora:

Prof. Dr. Luiz Henrique Capparelli Mattoso (EMBRAPA)

Profa. Dra. Alessandra de Almeida Lucas (UFSCar)

Prof. Dr. Hernane da Silva Barud (UNIARA)

O Relatório de Defesa assinado pelos membros da Comissão Julgadora encontra-se arquivado junto ao Programa de Pós-Graduação em Ciência e Engenharia de Materiais.

ACKNOWLEDGMENTS

- I would like to thank God for accompanying me and allowing me the opportunity to study at undergraduate and postgraduate programs;
- To my parents, Xia and Nian, for all their love, affection, support, encouragement and dedication;
- To the Federal University of São Carlos (UFSCAR), especially DEMa (Department of Materials Engineering) for the academic facilities and for welcoming me;
- To the company BioSmart in partnership with Dr. Hernane Barud for donating the bacterial cellulose used in this work;
- To Dr. Luiz Henrique Mattoso, not only for his guidance, but for all his personal and professional collaboration, which was very enriching;
- To Dr. Caio Otoni for his collaboration in the development of this research and, above all, for his help and patience with me during these two years;
- To Dr. Sebastião Canevarolo, for his friendship, advice and discussions that made several ideas in this work possible;
- To the other professors of the PPGCEM/UFSCar for the knowledge shared in classes and hallway conversations;
- To the PPGCEM secretariat for their patience, guidance and organization of the bureaucratic part of the work;
- To my friends at UFSCar for the laughs, the confessions and the help they never refused to give, including Vínicius Bacurau, Ana Larissa, Nícolas Moreira, Natália Silva, Victor Hugo, Caio Gueiros, Caroline Binde, Guilherme Stumpf, Marcos Vinícius and many others;
- To Embrapa Instrumentação for the research facilities;
- To CAPES - Coordenação de Aperfeiçoamento de Pessoal de Nível Superior for the financial support to carry out this work with a scholarship, process nº 88887.671697/2022-00.
- This study was financed in part by the Coordenação de Aperfeiçoamento de Pessoal de Nível Superior - Brasil (CAPES) - Finance Code 001.

ABSTRACT

The development of naturally occurring biodegradable materials has increasingly attracted the attention of researchers in recent years owing to the rising environmental concern. Among these materials, bacterial cellulose (BC) stands out as an easily obtainable polysaccharide mat with potential for application in several areas. Nanocelluloses, regardless of origin, are known to form gels in aqueous systems that, when dried, consolidate into materials stabilized both by the entanglements themselves and by hydrogen bonds between adjacent particles, the latter strongly dependent on the degree of interfibrillar orientation. Because of the above, this research aims to promote mechanical anisotropy at different levels through the preferential orientation of BC nanofibrils, achieved by asymmetric drying. The BC membrane was dried either in a “free” or “restricted” fashion within an atmosphere of controlled temperature and relative humidity. Different degrees of pre-stretching were also investigated to enhance the mechanical resistance and stiffness in the direction of the drying restriction. The resulting materials will be characterized concerning morphology, structure, and mechanical properties through scanning electron microscopy, polarized infrared spectroscopy, polarized optical microscopy, X-ray diffraction, and dynamic-mechanical thermal analysis. Promising conditions and potential applications will also be discussed and analyzed.

Keywords: Microbial cellulose; biocellulose; orientation; anisotropy.

RESUMO

PRODUÇÃO E CORRELAÇÕES MICROESTRUTURA–PROPRIEDADE EM MEMBRANAS DE CELULOSE BACTERIANA MONO-ORIENTADAS

O desenvolvimento de materiais biodegradáveis de origem natural tem atraído cada vez mais a atenção de pesquisadores nos últimos anos, devido à crescente preocupação ambiental. Entre esses materiais, a celulose bacteriana (CB) destaca-se como uma manta de polissacarídeo de fácil obtenção, com potencial para aplicação em diversas áreas. As nanoceluloses, independentemente de sua origem, são conhecidas por formar géis em sistemas aquosos que, quando secos, se consolidam em materiais estabilizados tanto pelos próprios entrelaçamentos quanto por ligações de hidrogênio entre partículas adjacentes, sendo estas últimas fortemente dependentes do grau de orientação interfibrilar. Diante disso, esta pesquisa tem como objetivo promover anisotropia mecânica em diferentes níveis por meio da orientação preferencial dasnanofibrilas de celulose bacteriana, obtida através de secagem assimétrica. A membrana de CB foi seca de forma “livre” ou “restrita”, em uma atmosfera com temperatura e umidade relativa controladas. Diferentes graus de pré-estiramento também foram investigados para aumentar a resistência mecânica e a rigidez na direção da restrição de secagem. Os materiais resultantes serão caracterizados quanto à morfologia, estrutura e propriedades mecânicas por meio de microscopia eletrônica de varredura, espectroscopia no infravermelho polarizado, microscopia óptica polarizada, difração de raios X e análise dinâmico-mecânica térmica. Condições promissoras e potenciais aplicações também serão discutidas e analisadas.

Palavras-chave: Celulose microbiana; biocelulose; orientação; anisotropia.

INDEX

TABLES

FIGURES

SYMBOLS AND ABBREVIATIONS

ASTM: American Standard for Testing of Materials

α: Alfa

β: Beta

μm: Micrometer

Δn: Birefringence

BC: Bacterial cellulose

DR: Dichroic ratio

DMTA: Dynamic mechanical thermal analysis

OPD: Optical path difference

PFTIR: Polarized Fourier-transform infrared spectroscopy

POM: Polarized optical microscopy

RH: Relative humidity

SEM: Scanning electron microscopy

XRD: X-ray diffraction

MPa: Megapascal

GPa: Gigapascal

BC_MO: Restricted dried BC without abrasive between the “claws”

BC_MO’:Restricted dried BC with abrasive between the “claws”

1 INTRODUCTION

The strong demand for the development of multifunctional sustainable materials with superior mechanical characteristics, large-scale and economically feasible production, and, ideally, derived from renewable resources is the result of rising environmental pressure over today's society (Li et al., 2021; Nechita et al., 2021). Biopolymers, which can replace conventional polymers made from non-renewable sources in a range of applications, have received particular interest in this context (A. C. Q. Silva et al., 2022). Among the most promising biopolymers for solid-state materials, cellulose stands out for its thermal and chemical stabilities and biodegradability, besides other technologically relevant features. Cellulose is a non-ionic, linear homopolysaccharide with 1,000–15,000 glucose units per chain, merged by β-1,4-glycosidic bonds. This naturally occurring polymer can be synthesized by plants, marine organisms, fungi, invertebrates, bacteria, and algae (He et al., 2020; Lahiri et al., 2021; Thomas et al., 2018).

Bacterial cellulose (BC) is a type of cellulose produced by certain bacteria that has been intensively investigated in recent years (Figure 1.1). BC has a unique nanostructure that is of high purity (i.e., devoid of lignin and extractives, as in plant cellulose), mechanical strength, biocompatibility, and biodegradability (Cacicedo et al., 2016; Li et al., 2021; Lin et al., 2020; Mbituyimana et al., 2021). Its nanostructure determines its physical and mechanical properties, allowing its conformation to be controlled by the type of cultivation and strategies that develop various morphologies, spatial structures, and functions (Wu et al., 2023).

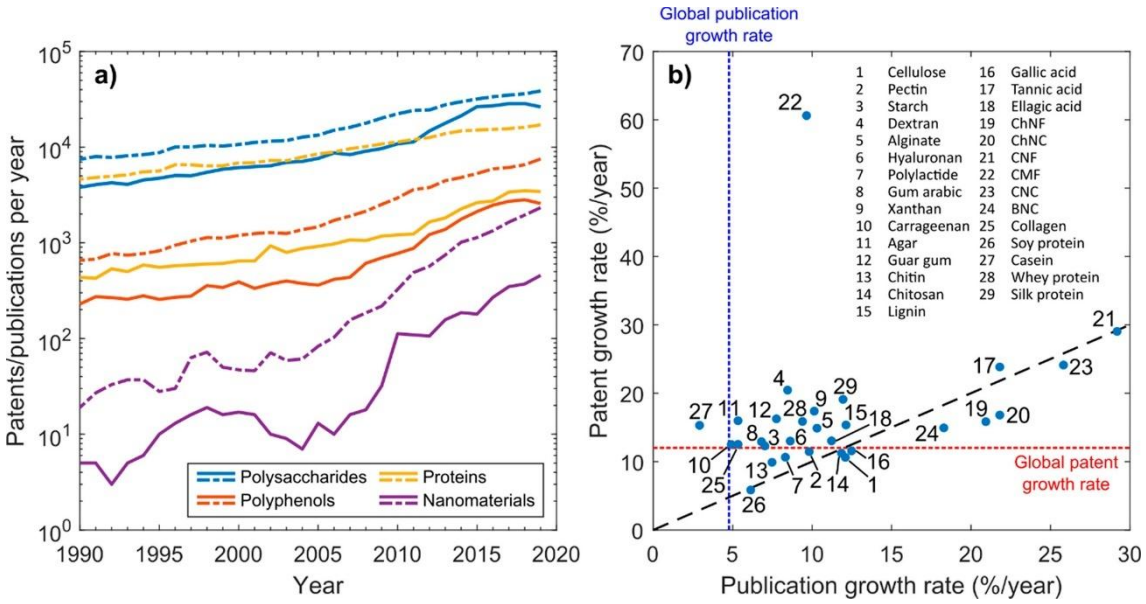

Figure 1.1: (a) Overview of the number of publications (dashed lines) and patents (continuous lines) per year published on biopolymers from 1990 to 2019. (b) Growth rate of patents and publications compared to the approximated global rates, used as reference. Note that one of the areas with the highest interest right now is bacterial nanocellulose (24). Reproduced from Tardy et al. (2021).

Physical hydrogels have recently been subjected by multiple types of drying procedures to study the effect of these protocols on the physiochemical properties of the material (Abral et al., 2021; Andree et al., 2021; Illa et al., 2019; Jiang et al., 2022; Prathapan et al., 2020a; S. Wang et al., 2017; Zeng et al., 2014). One of them is the convective drying, limiting one of the directions in which they can shrink, causing significant tensile stress to build along that route. This process has been observed to lead to the alignment of polymer chains within such an axis, influencing strength and toughness (Mredha et al., 2018). We herein intend to extrapolate this approach for wet BC membranes, aiming to promote the mono-orientation of the BC fibrils as well as to establish a robust relationship between the degree of anisotropy and other microstructural features and the macroscale properties of BC membranes dried in both ‘free’ and ‘restricted shrinkage’ conditions.

2 LITERATURE REVIEW

2.1 Cellulose

Cellulose is a linear homopolysaccharide consisting of β-D-glucopyranose units (anhydroglucose) linked by β-1,4-glycosidic interactions. It stands out for an estimated annual production of 10^{14} tons (Lima et al., 2015; Thomas et al., 2018). As demonstrated in Figure 2.1, the repeating unit of cellulose has a well-defined chemical structure. This biopolymer is highly valued for its numerous technological applications, attributed to its hydrophilic nature, chiral properties, biodegradability, and ability to undergo chemical modifications (Klemm et al., 2006). The molecular arrangement of cellulose facilitates the formation of a robust network through intermolecular hydrogen bonds and hydrophobic interactions, leading to the development of semicrystalline domains with a fibrous structuring that is insoluble in water and most organic solvents (Klemm et al., 2006; Medronho et al., 2012).

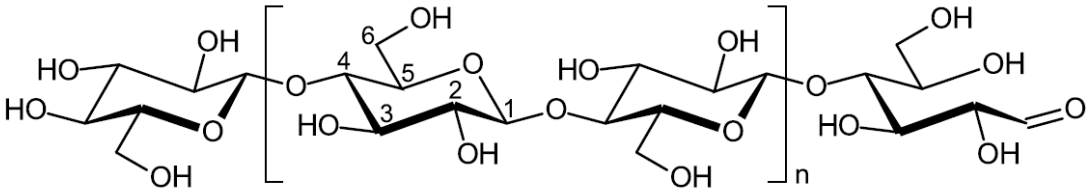

Figure 2.1: Structural representation of a cellulose chain.

Among other minor components, plant cell walls are made up of lignin, hemicelluloses, and cellulose, which make up roughly 30%, 30%, and 40%, respectively, of the plant biomass, although the ratios may vary based on the type of biomass and its growing conditions (Ek Monica et al., 2009).

Yet, besides plants, cellulose can be produced in the cells of various living things, including bacteria (such as *Acetobacter*, *Komagataeibacter*, *Rhizobium,* and *Agrobacterium*), fungi, algae, and marine animals, with different shapes and at high purity (Gandini & Lacerda, 2015; He et al., 2020; Lahiri et al., 2021). The cellulose produced by bacteria is referred to as native cellulose, and it comes in two crystalline forms, cellulose I and cellulose II, with cellulose I being the most

widespread. The glycan chains in cellulose I are oriented parallel to each other, while in cellulose II, they are arranged in an antiparallel fashion. Cellulose II is more stable due to an additional hydrogen bond per glucose chain (Brown Jr., 2004). The crystalline native cellulose (Figure 2.2) also has two subtypes, cellulose 1α and 1β, with cellulose 1β being more thermodynamically stable. The difference between these subtypes lies in how the hydrogen bonds are arranged in the chains close to the cellulose molecule. The ratio of 1α to 1β depends on the source of cellulose (Fink et al., 1997).

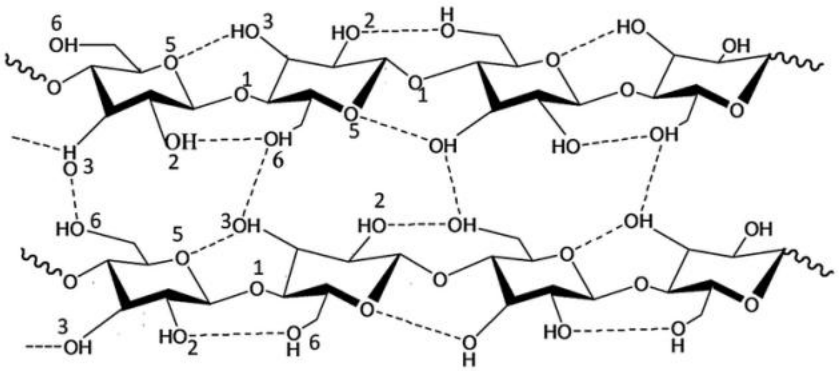

Figure 2.2: Schematic representation of the cellulose I chains, in the same plane. Source: Yuan; Cheng (2015).

2.2 Bacterial cellulose: Biosynthesis, Properties, and Applications

2.2.1 Biosynthesis

Bacterial cellulose (BC) was first described in 1886 by Brown, who was working with acetic acid bacteria. He identified a gel-like layer formed on the surface of vinegar fermentation broth, consisting of an extracellular gel material chemically equivalent to the cellulose in cell walls, and designated it as *Acetobacter xylinum* (Brown, 1886). This species, belonging to the family Acetobacteriaceae, has undergone several taxonomic reclassifications, and is now known as *Komagataeibacter xylinus* (Yamada et al., 2012). BC is aerobically generated in an aqueous culture medium containing sugar as a carbon source. It is produced as spheres, pellets, or irregular shapes under agitated culture or as

a sheet on the surface of the culture medium under static culture (Singhsa et al., 2018; J. Wang et al., 2019). The production time ranges from several days to weeks (Gatenholm & Klemm, 2010).

BC is typically produced under static culture and undergoes aerobic fermentation to form a gel-like layer that remains on the surface of the medium and has a high water-retaining capacity (Li et al., 2021). However, this more integrated process has low productivity and high cost as it requires a lot of time, a large surface area, and expensive raw materials, making its scaling-up difficult in the industry (Islam et al., 2017). As such, several strategies have been investigated to find new production lines to improve agitation and aeration (Czaja et al., 2004; Shavyrkina et al., 2021; Singhsa et al., 2018) and use cheaper carbon sources (Hong et al., 2012; Raiszadeh-Jahromi et al., 2020).

The composition of the culture medium varies according to the bacterial strain. The medium is essentially composed of a carbohydrate source (sucrose, glucose, fructose, lactose, mannitol, etc..), yeast extract, a nitrogen source (e.g., (poly)peptone, tryptone), and additives, as per Table 2.1.

Table 2.2.1: Different microorganisms and additives in the culture medium used to produce bacterial cellulose.

Microorganisms	Additives	Reference
Gluconacetobacter. medellensis	Glucose, sucrose, and fructose	(Castro et al., 2012)
Komagataeibacter xylinus **(ATCC 11142)**	Glucose	(Dhar et al., 2019)
Gluconacetobacter xylinus	Cotton cloth hydrolysate	(Hong et al., 2012)
Gluconacetobacter xylinus	Cashew apple juice and soybean molasses	(Souza et al., 2020)
Acetobacter xylinum **(ATCC 700178)**	Carboxymethylcellulose	(Cheng et al., 2011)
Gluconacetobacter hansenii **UCP1619**	Sugarcane molasses and acetylated glucose	(Costa et al., 2017)

2.2.2 Properties

BC is a naturally occurring biopolymer with remarkable properties, making it an attractive material for various applications. Unlike plant cellulose, BC is highly hydrated and devoid of lignin, pectic, hemicelluloses, and extractives. It

has superior mechanical properties due to its high crystallinity (84-89%) and unique fiber-forming capabilities (Li et al., 2021; Mbituyimana et al., 2021).

BC boasts a high-water vapor transmission rate and liquid sorption capacity due to its high hydrophilicity and capillarity induced by pores that are uniformly distributed between 10 and 300 nm. Also, cellulosic structures are often amphiphilic because of their extensive hydrogen bonding, associated with the crystalline organization of their chains, which leads to hydrophobic interactions. (Cacicedo et al., 2016; Lin et al., 2020; Mbituyimana et al., 2021).

The mechanical properties of BC membranes are also impressive (Table 2.2), with a high Young's modulus (15-35 GPa) and tensile strength (200-300 MPa). Other important features, including a high oxygen barrier, high thermal and chemical stabilities, biocompatibility, and non-toxicity, further enhance the potential of BC as a versatile material. In fact, native BC has been shown to support human cell growth, with over 70% proliferation of L929 fibroblast and osteoblast cells (LIN et al., 2020; Naomi et al., 2020).

Table 2.2.2: Mechanical properties of bacterial cellulose membrane and other polymeric materials in the literature.

Material	Young's modulus (GPa)	Tensile strength (MPa)	Elongation at break (%)	Reference
Bacterial cellulose	Up to 15-35	200-300	1.5-2.0	(Marestoni et al., 2020)
Polypropylene (PP)	1-1.5	30-40	100-600	(BARUD, 2010)
Highly oriented PP	~15	~450	~7	(Alcock et al., 2009)
Biaxially oriented PP	3.4	185.7	79.2	(Lepers et al., 1999)
Poly(ethylene terephthalate) (PET)	3-4	50-70	50-300	(BARUD, 2010)
Biaxially oriented PET	5.26	174.4	50	(Lepers et al., 1999)
Cellophane	2-3	20-100	15-40	(BARUD, 2010)
Epoxy	3-5	30-90	20-85	(BARUD, 2010)
Nylon™ 12	1-2	40-50	>200	(BARUD, 2010)

2.2.3 Applications

The high purity of BC and the peculiar properties mentioned above have aroused great interest in various areas, such as medicine (tissue engineering, implants, wound dressings), food (dietary fibers and food packaging), electronics (electronic paper, capacitors), and many others (Choi et al., 2022).

Regarding biomaterials, BC can be made highly porous and biocompatible, promotes tissue regeneration and better cell interaction, and can withstand high loads and abrasion (Hussain et al., 2019). BC can replicate the skin surface and create an ideal environment for wound healing (Ahmed et al., 2020; Lee et al., 2017). Similarly, implants have also been made using BC for urethra (Maia et al., 2018), cornea and retina (Binder et al., 2007; C. Zhang et al., 2020), bones (W. Zhang et al., 2020), and nerves (Yang et al., 2018).

The main reason BC has been studied in pharmacology is its potential for controlled drug release. BC membranes serving as wound dressings have demonstrated a high drug adsorption and transport capacity, enabling precise drug release and retention to boost treatment efficacy (Navya et al., 2022; Trovatti et al., 2012). BC can also be used as a subcutaneous implant for prolonged drug release (N. H. C. S. Silva et al., 2014; Trovatti et al., 2012). In addition to its uses in the skin, BC can be employed as a hydrogel for controlled drug release that is also activated by pH changes (Arikibe et al., 2019; Pandey et al., 2014)

BC can serve as a base for some food formulations in the food industry and be a suitable alternative for food packaging materials (Amorim et al., 2022; Shi et al., 2014). BC can be used as additives to replace fat (carbohydrate- or protein-based fat replacers) to produce “low-fat” foods (Guo et al., 2018; Marchetti et al., 2017). Similarly, BC can be used as a matrix to create artificial meat with a texture comparable to real meat (Marchetti et al., 2017).

For the electric and electronic industries, BC can provide a very alluring product. BC composites have the potential to serve as the foundation for producing OLEDs for flat and flexible video panels and electronic paper (Legnani et al., 2019; Tajima et al., 2020; Ummartyotin et al., 2012). Due to its dimensional stability, BC is utilized in speaker and headphone diaphragms because it offers great sound velocity over a wide range of frequencies (Yamanaka et al., 1989).

2.3 Optical property and birefringence of a material

When light interacts with an object, it can happen in a variety of phenomena, including diffraction, absorption, and scattering. It is well known that if light falls on the material, there is little chance of occurring absorption when electromagnetic radiation frequencies significantly differ from the resonance frequency of the medium's molecules. This can lead to deformations of the molecules' electronic clouds, or polarization. As a result, they begin to oscillate in a direction and at a frequency comparable to the incident light. As a result of this interaction, the molecules emit light with the same properties as the incident light, which also affects the surroundings. This effect reduces the speed of light propagation, and by correlating the relationship between the reduced speed and the speed of light in a vacuum, we can calculate the material's refractive index. The basic equation for the refractive index is represented by Equation 2.1, where n represents the index of refraction, c is the speed of light in a vacuum (3,0.108 m/s), and v is the speed of light in the medium (Sliney, 2016).

$$n = \frac{c}{v} \quad \text{(Equation 2.1)}$$

In addition, materials can be classified as isotropic or anisotropic depending on how their properties behave in a specific direction; for example, the presence of different mechanical properties in different directions gives us an anisotropic material, the opposite is classified as isotropic (the same properties in all directions), this also occurs for interactions with light. Therefore, two primary optical properties are used to characterize the presence of anisotropy or isotropy in a material: dichroism and birefringence.

Dichroism is the property of absorbing electromagnetic radiation incident on the material in a specific direction and is orientation dependent. On the other hand, birefringence occurs when electromagnetic radiation hits a material, and it has two refractive indices (or double refraction) (Hecht, 2002). When light propagates in an optically anisotropic material, two rays with perpendicular

polarization states are formed, which travel through the material at different speeds and in different directions. The wave whose electric field is oriented perpendicular to the optical axis of the material is called an ordinary ray, while the one oriented parallel to it is classified as an extraordinary ray (figure). In this way, the ordinary ray is associated with a refractive index, n_o, and the extraordinary ray to another, ne (Figure 2.3).

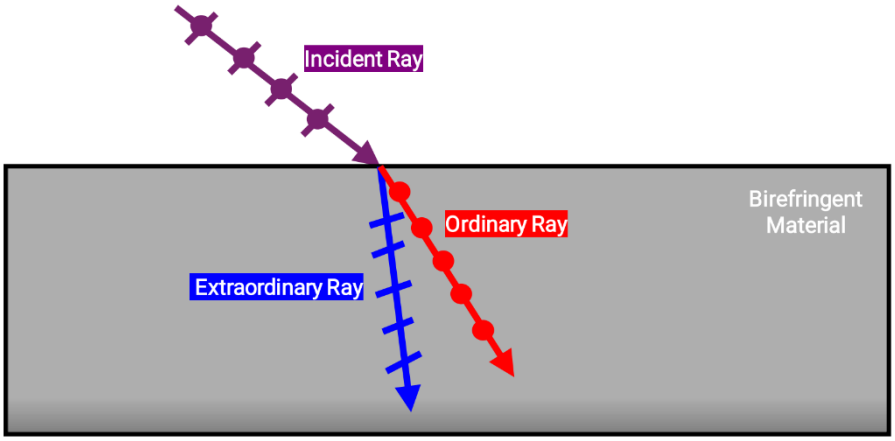

Figure 2.3: Schematic representation of the interaction of light in a birefringent medium.

Thus, the birefringence (Δn) is determined by the difference between these two refractive indices:

$$\Delta n = n_e - n_o \quad \text{(Equation 2.2)}$$

Hence, this optical property is commonly used to observe the orientation and anisotropy in several fields, like biology, geology (Jin et al., 2024), and polymer science (Medhat et al., 2017; van Aken & Janeschitz-Kriegl, 1980; Yu et al., 2021). In geology, it is commonly used to identify a mineral by using the interference colors (ZHOU; STARKEY; MANSINHA, 2004), and a more advanced is in the shear wave splitting, often referred to as seismic birefringence, is one of the best geophysical methods for identifying mantle flow fields in

mineralogy through the detection of seismic azimuthal anisotropy in the Earth's upper mantle. This method is especially useful in tectonically active areas, including subduction zones, where seismic activity can be significantly influenced by the mantle's movement and flow (Jin et al., 2024). In biology, you can directly understand the dynamics and structure of molecular organization in systems like striated muscles, protein solutions, and other biological systems by measuring the birefringence in living cells. (Katoh et al., 1999; Taylor & Cramer, 1963). Finally, in polymer science, the repeating unit is considered optically anisotropic due to the direction-dependent interactions between the light and the electronic cloud of the atoms. However, when the polymer molecules have a random conformation, the anisotropy of the polymer chains is canceled out, and the polymer becomes isotropic (Tagaya & Koike, 2001). On the other hand, when polymers are subjected to a deformation process, the chains are organized in the direction of flow, which consequently causes anisotropy in the region subjected to this stress field (Inoue, 2021). In this way, we use this property to study orientation, crystallization kinetics, and residual stresses, for example, in injected parts. When analyzed between crossed polarizers, these anisotropic materials are easily identified compared to optically isotropic materials. Unlike anisotropic materials, isotropic materials are characterized by the fact that light always travels at the same speed in any direction and vibrates in all directions perpendicular to the direction of propagation, so they take on a black color (extinct color) at any position in relation to the crossed polarizers.

2.4 Orientation and anisotropy

Polymers tend to align themselves in the direction of flow or deformation during numerous industrial processes like drawing, extrusion, injection molding, and rolling. The literature has extensively examined and reported on this phenomenon (Bartczak et al., 2002; Gao et al., 2021; Gibson & Ward, 1980; Nakayama & Kanetsuna, 1975). The resulting mechanical anisotropy is an important element in determining the yield and failure behavior of materials. The changed tensile stress that polymer samples encounter when tested at different angles in relation to their orientation direction is one of the most important

manifestations of this effect. Many investigations on this subject have described the impact of anisotropy on the mechanical characteristics of materials. These discoveries significantly impact the creation of new materials and improved industrial processes.

Similarly to other materials, BC can be modified physically through stretching (Jiang et al., 2022; Zhao et al., 2022). These processes may result in the structural collapse or loss of micropores with a few microns diameter. This can enhance the interfibrillar orientation into a denser association or further increase their mechanical strength, enabling applications wherein this asset is demanded.

3 OBJECTIVES AND HYPOTHESES

3.1 General objective

The central scientific hypothesis guiding this research was that the uniaxial restriction of the volumetric contraction experienced during drying would be able to induce preferential orientation amid BC fibrils in the direction of the restriction, raise the degree of interfibrillar interaction, generating mechanical anisotropy, and ultimately lead to greater resistance in the direction parallel to the orientation. This project was then intended to promote BC interfibrillar mono-orientation, as well as to establish relationships between the degree of anisotropy and other microstructural characteristics and the macroscale properties of BC membranes dried in “free” and “restricted” fashions in terms of shrinkage, with the goal of increasing mechanical resistance and stiffness in the direction of the drying restriction.

3.2 Specific objectives

- Follow the microstructural evolution of wet BC mats during “free” and “restricted” drying;
- Establish correlations between the mechanical and structural properties of dried BC membranes with the degree of anisotropy induced by the different drying protocols;
- Produce oriented BC membranes with anisotropic mechanical properties;
- Validate or refute the primary scientific premises that support this dissertation.

4 MATERIALS AND METHODS

4.1 Preparation of bacterial cellulose membranes

The BC mats were supplied by BioSmart Nanotechnology after being produced as described by Breijaert et al. (2025) using the bacterium Komagataeibacter rhaeticus on Hestrin-Schramm (HS) agar in an air-circulating oven at 28 °C for 24 h. Briefly, the third inoculum of the microorganism was grown for 72 h at the same conditions as before but in an Erlenmeyer flask containing the HS culture medium made up of 50 g glucose, 4 g yeast extract, 0.73 g magnesium sulfate, 2 g potassium phosphate, 20 mL absolute ethanol 99.8%, and 980 mL distilled water. The BC membrane formed at the interface between the culture medium and the atmosphere was purified with 0.1 M sodium hydroxide (NaOH) solution in a water bath at 70-80 ºC for 30 min and then thoroughly washed with distilled water until pH neutrality was achieved, aiming to remove bacterial cells.

4.2 Free and uniaxially restricted drying of BC membranes

To assess the volumetric contraction experienced during the supposedly "free" of constraints, the wet BC membranes were shaped into rectangular geometries of 100 mm in length and 10, 30, or 50 mm in width and dried at room temperature and relative humidity (RH) of 20% controlled by silica gel inside a desiccator. Wet membranes with the same geometries were also dried with uniaxial restrictions, as indicated in Figure 4.1 so that volumetric contraction was only permitted in the direction perpendicular to the constrained axis. To evaluate the impact of these independent variables on the microstructural and macroscopic features of the dried membranes, this restricted drying was also carried out at different stretching levels, enabled by the movable clamps of a device designed by our research group (Figure 4.2). Afterward, selected films were characterized to establish statistical relationships between film dimensions and shrinkage percentages during drying.

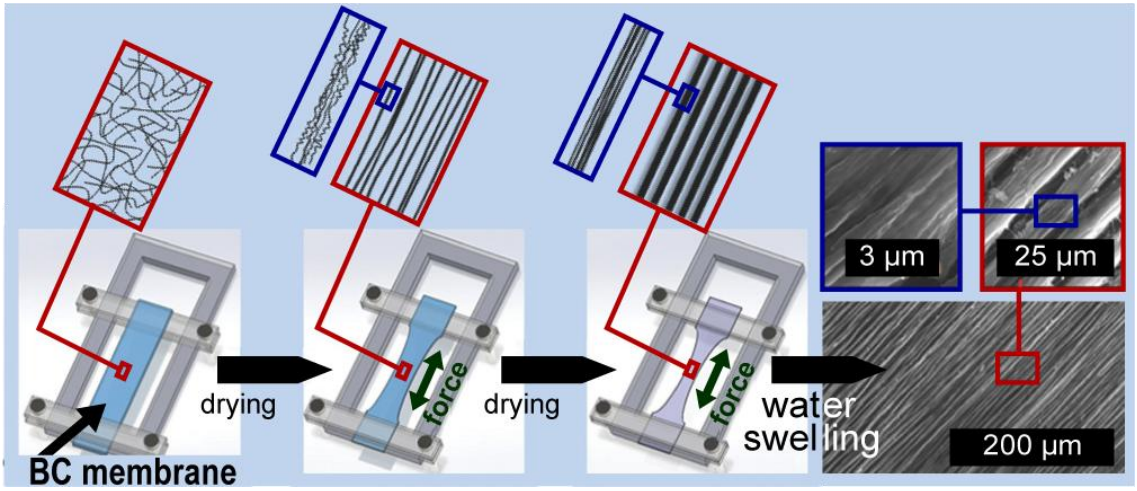

Figure 4.1: Schematic illustration of the apparatus used for drying the wet BC membranes with uniaxially restricted contraction. It is expected that the nanofibrils, previously randomly oriented (left), are gradually oriented in the direction parallel to the constraint (right), depending on the level of stretching and the capillarity experienced under different conditions of temperature and relative humidity. Adapted from Mredha et al. (2018).

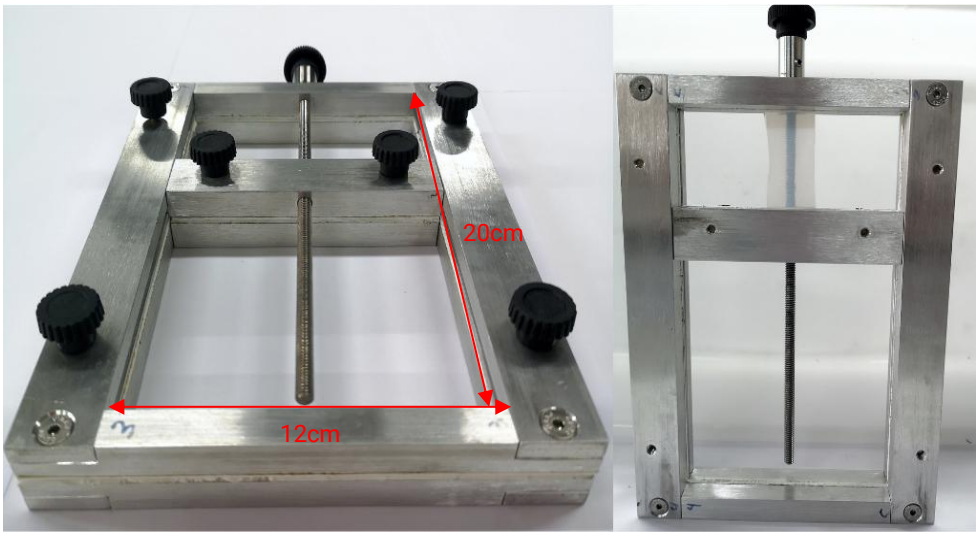

Figure 4.2: Device with movable clamps designed by the group (left) and an example of a BC membrane drying in a uniaxially restricted direction (right).

4.3 Polarized Fourier-transform infrared spectroscopy (pFTIR)

The pFTIR spectra were obtained on a Nicolet 6700 from Thermo Scientific spectrometer operating with polarized IR light under the following conditions: percentage of absorbance (1/T) with an accumulation of 64 scans, with a resolution of 4 cm^{-1}, in the wavenumber absorption range from 4000-400 cm^{-1}. Each spectrum from pFTIR was normalized with OriginPro. This method used the dichroism feature of anisotropic materials, which occurs when light with various polarizations is absorbed at different rates. This showed the variation in absorbance peak intensities at various polarization angles. The spectra acquired at perpendicular and parallel polarizations of the entering light were used to determine orientation. While no change in the intensity of bands is seen for a random material, the peak absorbance intensities at two mutually perpendicular polarizations are expected to vary for an oriented material. The dichroic ratio (DR), which is the ratio of the intensities of the light polarized parallel and perpendicular to the fiber direction ($DR = A_{//} / A_{\perp}$), was used to determine the degree of alignment (Kakade et al., 2007). We relied on this method to gain insight into the orientation of BC fibrils from the DR after they are dried. Previous studies examined the DR from the absorption bands 1,160 cm^{-1} for cellulose fibers (Belbachir et al., 2011; Kafle et al., 2017). This band was attributed to the coupling of the stretching vibrations of C-O-C and, therefore, was also used in this study.

4.4 Scanning electron microscopy (SEM)

The morphologies of the membranes dried under different conditions described above were investigated by SEM after being coated with a layer of platinum through cathodic sputtering on ZEISS DSM 960. Surface and cryo-fractured cross-sections (in both machine/parallel and transverse directions) were imaged. After that, the images were analyzed by two existing plugins in the ImageJ software, which aim to infer the preferred orientation of the samples in the SEM input image. It computes a histogram that indicates the number of structures (fibers, tubes, etc.) in each direction. It also reproduces the analyzed image with the directions/angles in which orientations are found, represented by

colors from a color map. The images with isotropic characteristics are expected to show a flat histogram, whereas images with a preferred orientation are expected to give a histogram with a peak at that orientation.

4.5 Anisotropy analysis through crossed polarizer system and Michel-Levy color chart

The dried BC films were analyzed using a system of crossed polarizers that, in contact with the samples, made it possible to visualize the birefringence of the sample. Based on the spectrum color shown by the system, the Michel-Levy color charts were used to estimate the level of anisotropy.

4.6 X-ray diffraction (XRD)

The dry BC membranes were analyzed by XRD to elucidate their crystallographic patterns and degree of crystallinity. XDR-6000 diffractometer (Shimadzu) will be used with Cu-Kα radiation (λ = 1.5406 Å) and with 2θ ranging between 5º and 60º.

4.7 Mechanical properties

The dry BC membranes were subjected to dynamic mechanical analysis, using tensile film clamp configuration. Rectangular specimens were cut from the dried BC membranes, and to evaluate the mechanical anisotropy induced by the restricted drying process, they were carefully cut in two orthogonal orientations: (i) parallel (0°) to the uniaxial drying direction (machine direction, MD), and (ii) transverse (90°) to it (transverse direction, TD).

This preparation ensured that differences in stiffness and deformation behavior could be directly attributed to fibril alignment. The strain-rate mode was selected to control the deformation during testing. Before each run, the samples were equilibrated at 30 °C, followed by a strain ramp of 0.5%·min^{-1} up to a maximum strain of 50%. Experiments were carried out under an air atmosphere with continuous acquisition of stress (MPa) and strain (%). This procedure enabled the extraction and comparison of tensile modulus and stress–strain

responses between MD- and TD-oriented specimens, allowing a quantitative assessment of the mechanical anisotropy generated by the drying-induced fibril orientation.

5 RESULTS AND DISCUSSION

5.1 Drying procedure

The wet membranes were cut into three rectangular geometries (1x10, 3x10, and 5x10 cm^2 with an average thickness of 1,30 mm) and dried at three conditions. The first condition was the "free" drying, in which the dried films were not constrained in any direction (Figure 5.1). To achieve this, a non-stick baking sheet was used as a drying substrate. The second drying condition was achieved by restricting the axial direction of the sample, as seen in Figure 4.1; however, in this process, the BC membrane was not pre-stretched, as the sample was placed in such a way that it was only aligned with the axial axis of the frame. Finally, the last condition was the restricted drying in the axial direction of the frame with the application of pre-stretching. Each geometry and drying condition was obtained in three repetitions.

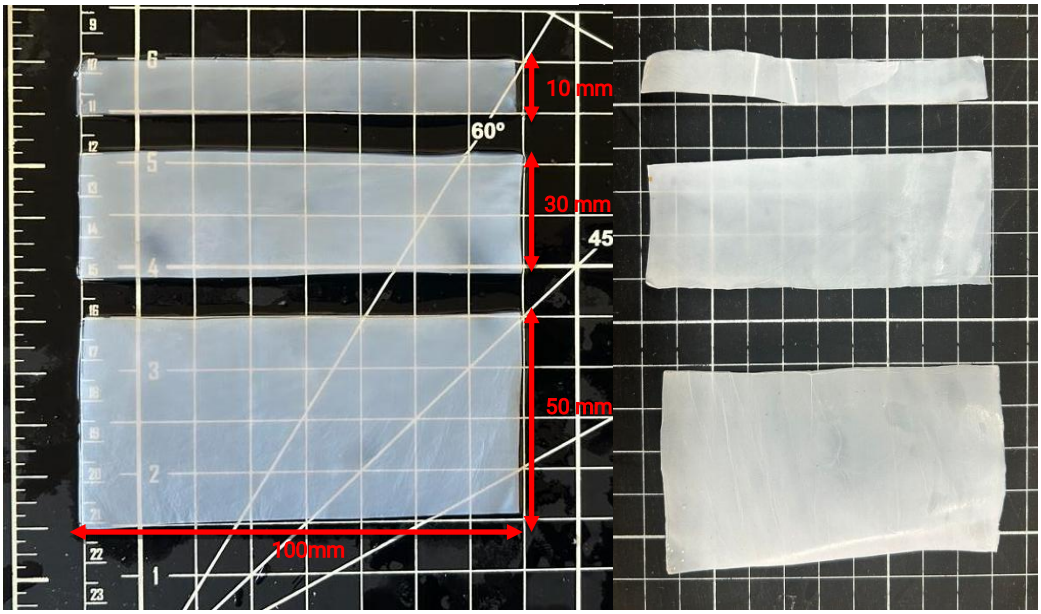

Figure 5.1: Images of the samples before and after the free drying.

5.1.2 “Free” drying

After collecting the samples in triplicate for each geometry, the percentage of shrinkage experienced during drying was determined based on the average

linear shrinkage for each dimension (length, width, and thickness). These values were treated in the Minitab statistical software for analysis of variance (ANOVA) at 5% significance to verify significant differences between the means of these three independent groups and the possibility of predicting shrinkage during drying. Whenever suitable, the ANOVA output was fed into a Tukey's post hoc test at p = 0.05 to investigate quantitative differences as per (Table 5.1). Concerning width, the shrinkage percentage was significantly different: the 50-mm-wide film shrank the most. However, necking was not observed as this type of drying did not lead to expressive anisotropic contraction, as expected.

Table 5.1: Percentage contraction in the three dimensions (length, width, and thickness) of bacterial cellulose mats after free drying. The lowercase letters refer to comparisons among values in the same column.

Original width (mm)	Length shrinkage (%)	Width shrinkage (%)	Thickness shrinkage (%)
10	2.7± 0.8 [a]	1.3 ± 0.5 [a]	72 ± 1 [a]
30	3.2 ± 0.3 [a]	1.5 ± 0.4 [a]	74 ± 3 [a]
50	3.6 ± 0.2 [a]	4 ± 2 [b]	72 ± 1 [a]

5.1.3 Restricted drying without pre-stretching

In this case, the samples were dried in the designed frame (Figure 4.2) to restrain one of the directional axes; however, during this drying process, no force was applied to pre-stretch the wet BC membranes, and the RH was controlled (20%) using silica gel. ANOVA was also carried out for the shrinkage percentage. As per Table 5.2, the specimen length was not reduced because it was constrained along the main axis. This, in turn, led to a necking effect in width, which also shrank more than in the “free” drying condition. Necking occurred unevenly and predominantly in the 10-mm-wide geometry.

Table 5.2: Percentage contraction in the three dimensions (length, width, and thickness) of bacterial cellulose mats after restricted drying without pre-stretching. The lowercase letters refer to comparisons among values in the same column.

Original width (mm)	Length shrinkage (%)	Width shrinkage (%)	Thickness shrinkage (%)
10	-	49 ± 8 [a]	81 ± 1 [a]
30	-	18 ± 3 [b]	81.5 ± 0.6 [a]
50	-	15 ± 3 [b]	80.4 ± 0.4 [a]

5.1.3 Restricted drying with pre-stretching

Pre-stretching the wet BC membranes before drying did not lead to thickness and length variations, unlike the width (Table 5.3). Again, the 10-mm-wide membrane showed a higher percentage of width reduction.

Table 5.3: Percentage contraction in the three dimensions (length, width, and thickness) of bacterial cellulose mats after restricted drying with pre-stretching. The lowercase letters refer to comparisons among values in the same column.

Original width (mm)	Length shrinkage (%)	Width shrinkage (%)	Thickness shrinkage (%)
10	-	64 ± 5 [a]	86.6 ± 0.6 [a]
30	-	38 ± 2 [b]	87.4 ± 0.8 [a]
50	-	30 ± 4 [b]	85 ± 1 [a]

From another perspective, ANOVA compared samples of the same geometries with different drying processes. Table 5.4 shows lowercase and

uppercase letters; the lowercase letters refer to comparisons among values in the same column, i.e., samples with different initial widths, while the uppercase letters pertain to a comparison by row, meaning for samples of the same initial width but dried under various conditions. Therefore, it is noted that for the material of the same width, under different drying conditions, the percentage reduction in the shrinkage of the BC film is exclusively different. Therefore, it was not possible to find a shrinkage pattern during drying, which we could use to control the necking of the material and thus obtain a perfectly rectangular material when dried.

Table 5.4: Width shrinkage of BC membranes of different geometries and dried differently. The lowercase letters refer to comparisons among values in the same column while the uppercase letters pertain to a comparison by row.

Original width (mm)	**Length shrinkage (%)**	**Width shrinkage (%)**	**Thickness shrinkage (%)**
10	1.3 ± 0.5 ^{aC}	49 ± 8 ^{aB}	64 ± 5 ^{aA}
30	1.5 ± 0.4 ^{aC}	18 ± 3 ^{bB}	38 ± 2 ^{bA}
50	4 ± 2 ^{bC}	15 ± 3 ^{bB}	30 ± 4 ^{bA}

Table 5.5: Thickness shrinkage of BC membranes of different geometries and dried differently. The lowercase letters refer to comparisons among values in the same column while the uppercase letters pertain to a comparison by row.

Original width (mm)	**Length shrinkage (%)**	**Width shrinkage (%)**	**Thickness shrinkage (%)**
10	72 ± 1 ^{aC}	81 ± 1 ^{aB}	86.6 ± 0.6 ^{aA}
30	74 ± 3 ^{aC}	81.5 ± 0.6 ^{aB}	87.4 ± 0.8 ^{aA}
50	72 ± 1 ^{aC}	80.4 ± 0.4 ^{aB}	85 ± 1 ^{aA}

5.2 Anisotropy analysis through crossed polarizers and Michel-Levy color chart

The anisotropy analysis was conducted using an instrument created from a simple white LED panel and two crossed-polarized films, as shown in Figure 5.2. The BC films, once dried, were placed in the apparatus to observe the change in birefringence caused by the different drying processes and then compare them to determine which BC film would have the higher anisotropy, degree of orientation of crystalline regions, or alignment of chains. As previously mentioned, the films subjected to this test were: the BC membranes dried “freely” (Figure 5.4), with restriction in their longer axis but without pre-stretching (Figure 5.5), and both restricted and pre-stretched (Figures 5.6 and 5.7). However, for the latter, different levels of pre-stretching were applied. For crystalline and amorphous polymers, the birefringence reflects the degree of orientation of crystalline regions or the alignment of chains under the influence of specific factors such as thermal treatment (annealing) and, in this case, mechanical stress (stretching) (Postolache et al., 2022).

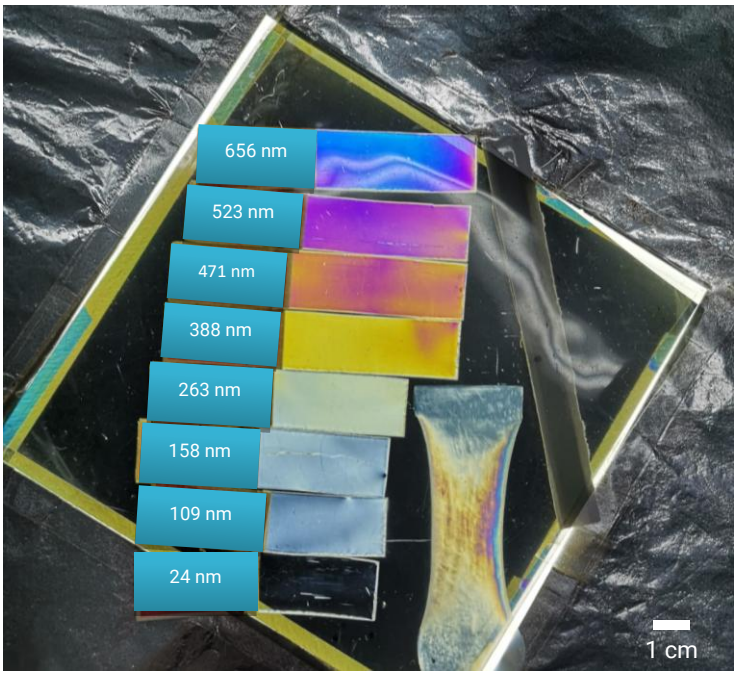

Figure 5.2: Image of the white LED panel with two crossed-polarized films sandwiching polyethylene films of different optical birefringences (for comparison purposes) and a representative BC dried film.

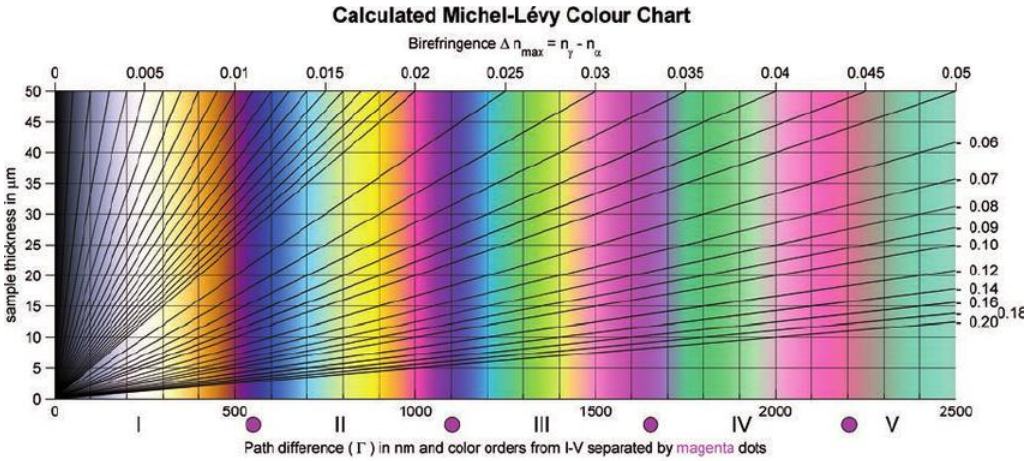

Figure 5.3: Michel-Lévy interference color chart, considering an average wavelength of 550 nm for white light. Adapted from (SØRENSEN, 2013).

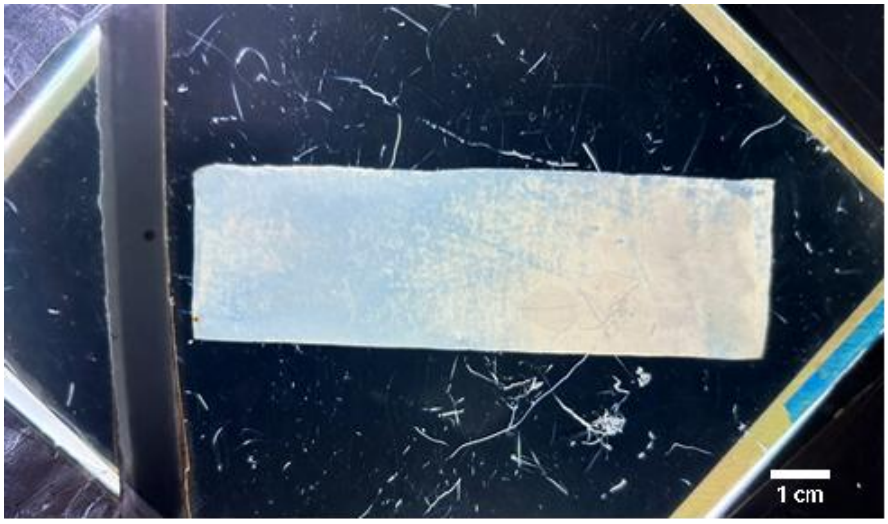

Figure 5.4: Digital Image of a BC film dried in a “free” fashion within crossed polarizers.

With regard to the BC membranes that were dried but fixed in the axial direction (Figure 5.5), even though they were restricted in one direction, there was no significant difference in their birefringence, as per the white (1st order) to

yellowish-white color transition, which means that there was an increase in birefringence, but there was no considerable increase in anisotropy.

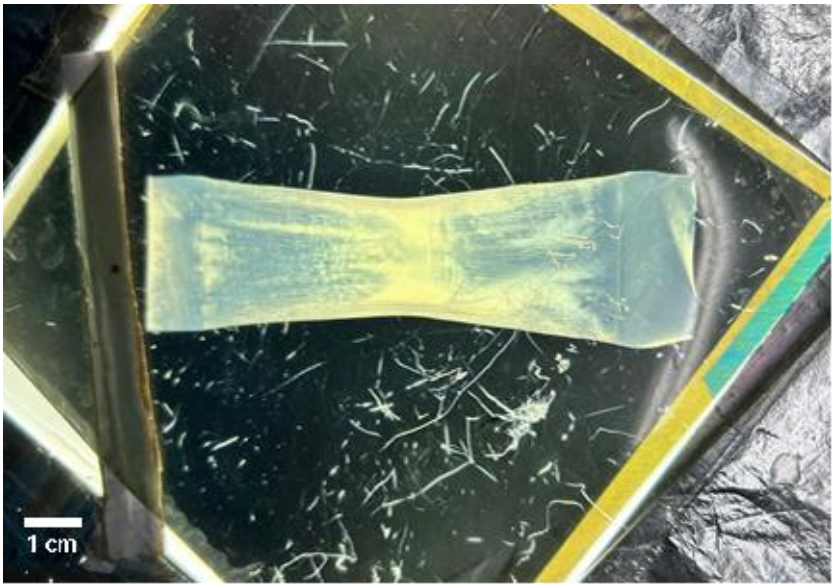

Figure 5.5: Image of a sample restricted dried in the axial axis without the pre-stretching inside the crossed polarizers system.

For the BC mat dried in a restricted, pre-stretched way, there were some difficulties during drying: when the BC was subjected to pre-stretching, it slipped out of the frame, preventing it from drying expectedly; also, the pre-stretching could be applied to the polymer without it slip was low so it allowed the chains that were oriented due to stretching to relax during drying, resulting in a polymer similar to ordinary BC. To solve these problems, two simple ways were used to see which would be the most advantageous to induce orientation in the uniaxial direction of the BC microfibrils. The first was to increase the contact area of the BC with the "claws"; in other words, the proper length of the BC film was reduced by clamping a larger area in the restriction zone (the ends of the films). The second way was to use polishing sandpaper attached to the ends of the samples when drying to increase friction due to contact between the protrusions of the sandpaper and the film, promoting the possibility of applying a greater pre-stretch to the film. The two methods were used, and the results can be seen in Figures 5.6 and 5.7, respectively. In both, it was possible to notice a change in optical

anisotropy and, therefore, an increase in birefringence. The BC in Figure 5.6 shows maximum second-order birefringence due to its coloration, which goes from yellow in the first order and tends to dark blue in the second. In contrast, Figure 5.7 shows the passage of interference colors up to the yellow of the second order, thus representing a higher value of birefringence. Hence, the sample has a higher value of optical anisotropy. Therefore, the drying procedure provokes a theoretical increase in the degree of orientation or alignment of the chains. It can be confirmed using other techniques to analyze their orientation, like SEM and pFTIR.

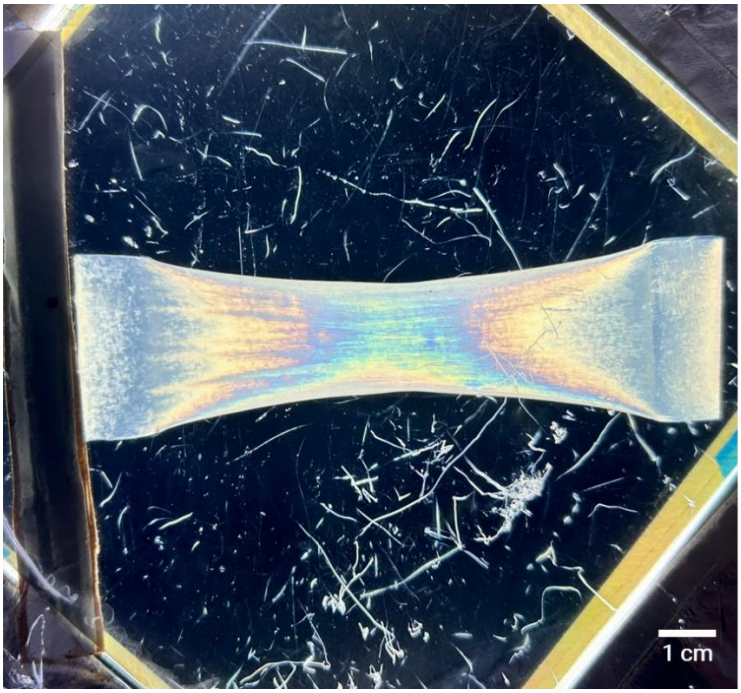

Figure 5.6: Image of a sample restricted dried in the axial axis with pre-stretching inside the crossed polarizers system.

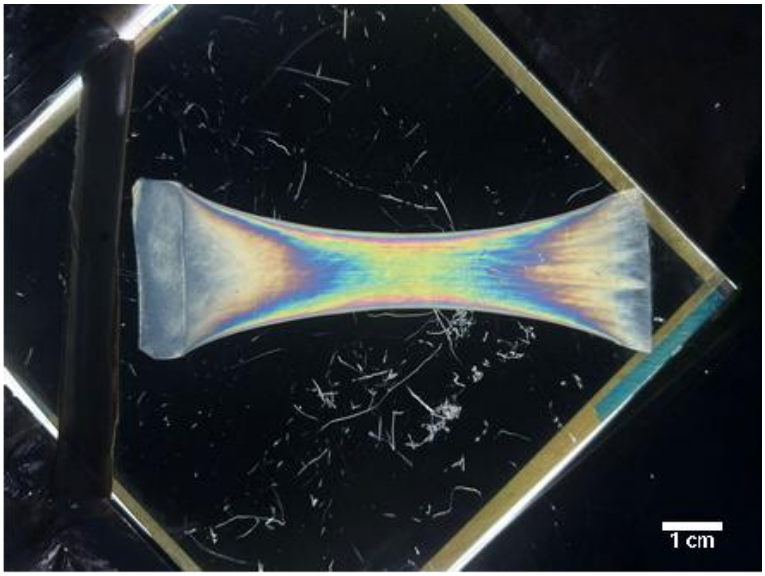

Figure 5.7: Image of a sample restricted dried in the axial axis with pre-stretching inside the crossed polarizers system. Using an abrasive to get more fixation in the frame “claws.”

5.3 Polarized Fourier-transform infrared spectroscopy (pFTIR)

After characterizing the BC using birefringence to verify the optical anisotropy and estimate the degree of orientation in the axial direction of the frame, pFTIR, which uses the dichroism property of a material, was applied to verify the presence of orientations, further validating the previous results. To do this, an attenuated total reflectance FTIR was first carried out to check for the presence of the valence bands shown in Figure 16.

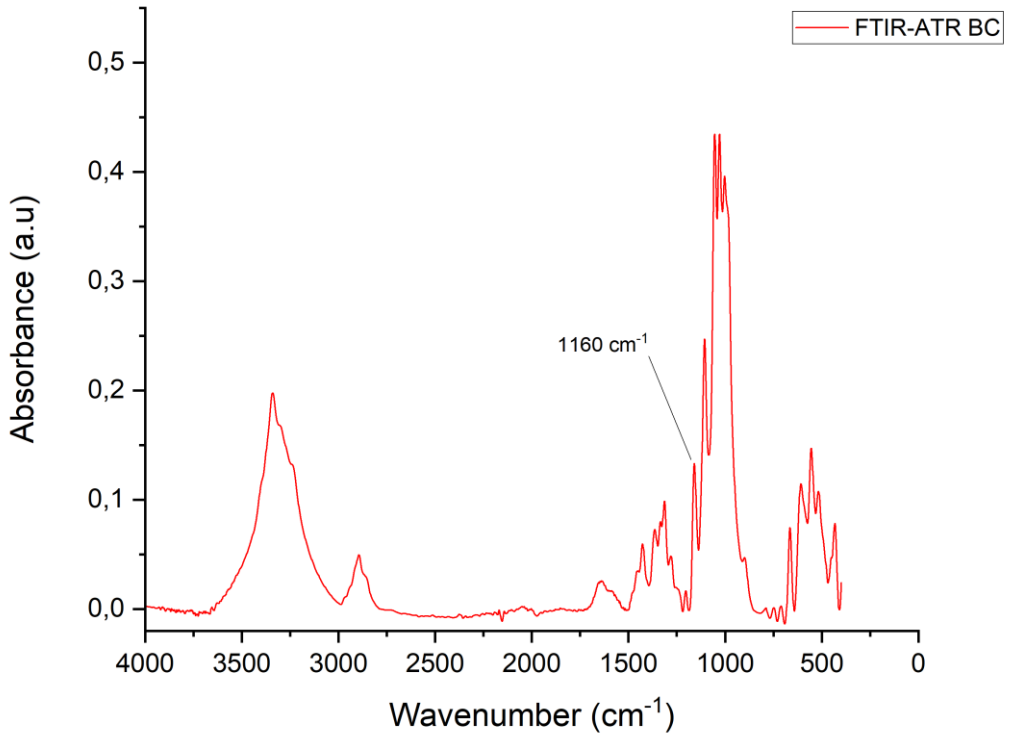

Figure 5.8: ATR-FTIR spectrum of a bacterial cellulose film dried “freely.”

The absorption band around 1160 cm^{-1} has been highlighted for better visualization as it was used to calculate the dichroic ratio, as in previous studies (Belbachir et al., 2011; Kafle et al., 2017; Kakade et al., 2007). The absorption bands in Figure 5.8 are characteristic of cellulose, where the bands between 3000-3700 cm^{-1} are attributed to the stretching vibration bands of the O-H bonds of the primary and secondary hydroxyl groups; the band around 2900 cm^{-1} is attributed to the stretching vibration of the C-H bond; that at ~1650 cm^{-1} represents adsorbed water, i.e., also O-H bonds; those centered at 1315, 1335, 1430, and 1470 cm^{-1} are correlated to the in-plane bending vibration bands of the primary and secondary hydroxyl groups; the band at ~1160 cm^{-1} is attributed to the anti-symmetric stretching vibration of the C-O-C glycosidic bond; those at 1110, 1060, and 1035 cm^{-1} are assigned to the vibrations of the C-O bond of carbons 2, 3, and 6; finally, the bands at 665 and 705 cm^{-1} are due to out-of-plane

torsional vibrations of hydrogen-bonded O-H groups (Atykyan et al., 2020; Foster et al., 2018; Kafle et al., 2017).

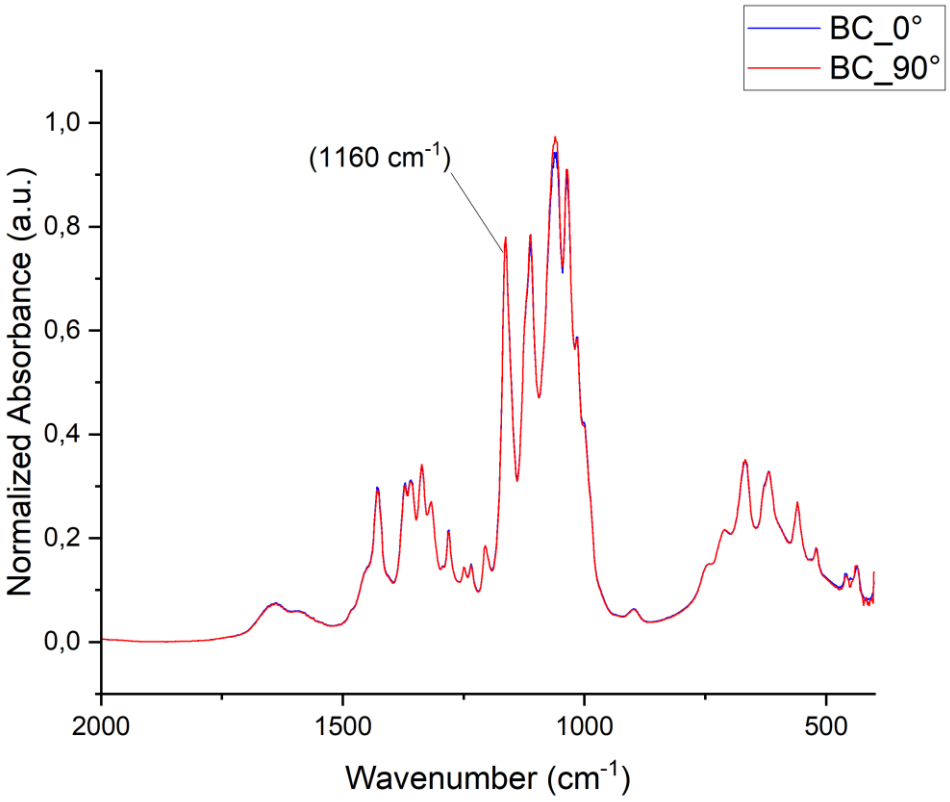

Figure 5.9: pFTIR of “freely” dried bacterial cellulose films parallel (blue) and perpendicular (red) to the constrained direction.

Coupling cross polarizers to a FTIR operating in transmission mode allows observing the behavior of the bands assigned to the material in a particular direction, which in turn enables studying the orientation of the polymer chain using dichroism. In this sense, Figures 5.9 and 5.10 evidence that the absorption profile in natural BC differs from that in pre-stretched BC. Figure 5.9 shows that the absorbance values at ~1160 cm^{-1} in the "freely" dried BC are slightly higher in the perpendicular direction (90°) than the parallel direction (0°), leading to a dichroic ratio (DR) of 0,99. Because this value is close to 1, this sample is considered non-oriented. This deviation from isotropy, meaning a slight preferential orientation, is assigned to the intrinsic birefringence of BC. The

literature shows that the preferential orientation of cellulose microfibrils for the band studied is around 30° (Kafle et al., 2017).

On the other hand, Figure 5.10 shows the spectra recorded in restrictedly dried BC that has been pre-stretched with no abrasive clamps, evidencing a much more pronounced difference compared to the previous behavior. The absorbance value of the parallel peak is higher than in the perpendicular direction, pointing to a certain level of orientation (DR = 1.20). This low DR corroborates the low birefringence shown in Figure 5.6. Still, DR > 1 surpasses the intrinsic birefringence of BC itself and reflects the orientation arising from the restricted drying scheme.

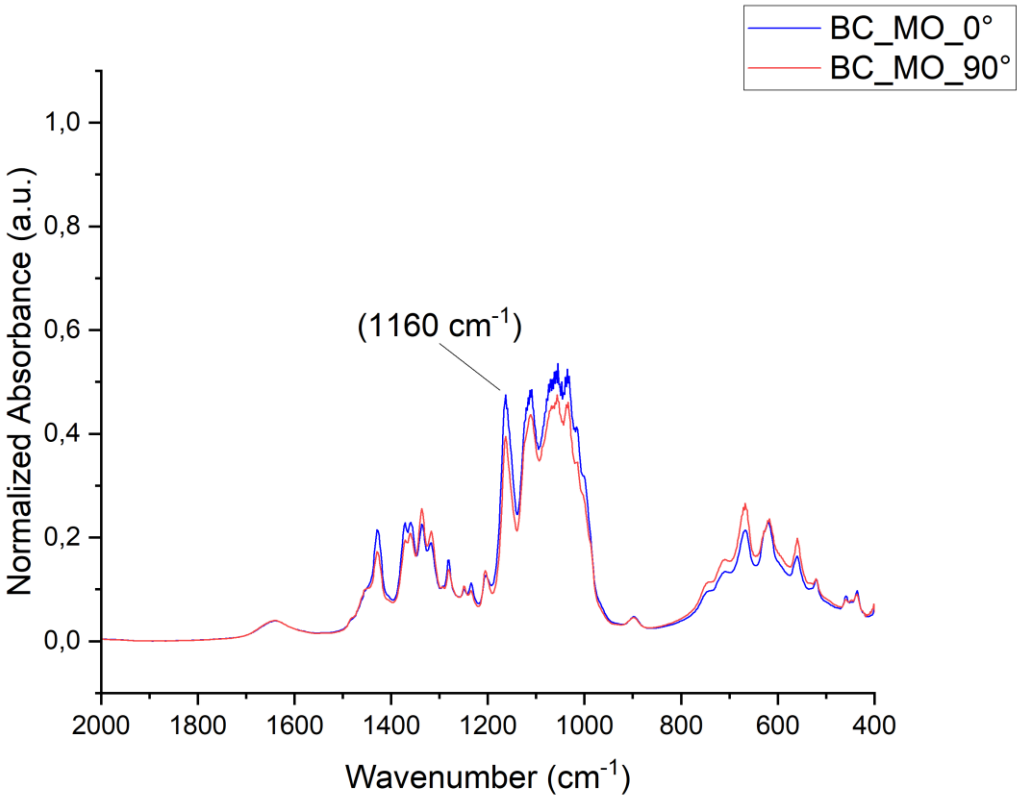

Figure 5.10: pFTIR of restricted BC with pre-stretching but without the abrasive in the parallel (blue) and perpendicular (red) of the constrained direction.

The spectra of the most birefringent samples (i.e., restrictedly dried and pre-stretched by abrasive clamps) is shown in Figure 5.11. We needed to deal

with a common error in transmission FTIR testing where the absorption bands fall beyond the Beer-Lambert-Bouguer limit, i.e., the absorption value exceeds one unit. This causes unreliability in the characterization resulting in biased absorbance, deviating from the linearity. This can be caused by various phenomena, for example, high sample thickness, which can be the case for shrank samples. To solve this, an adhesive tape was used to tear off a thin strip of the dried BC film, enabling one to observe an increase in orientation that led to a DR of 1.33.

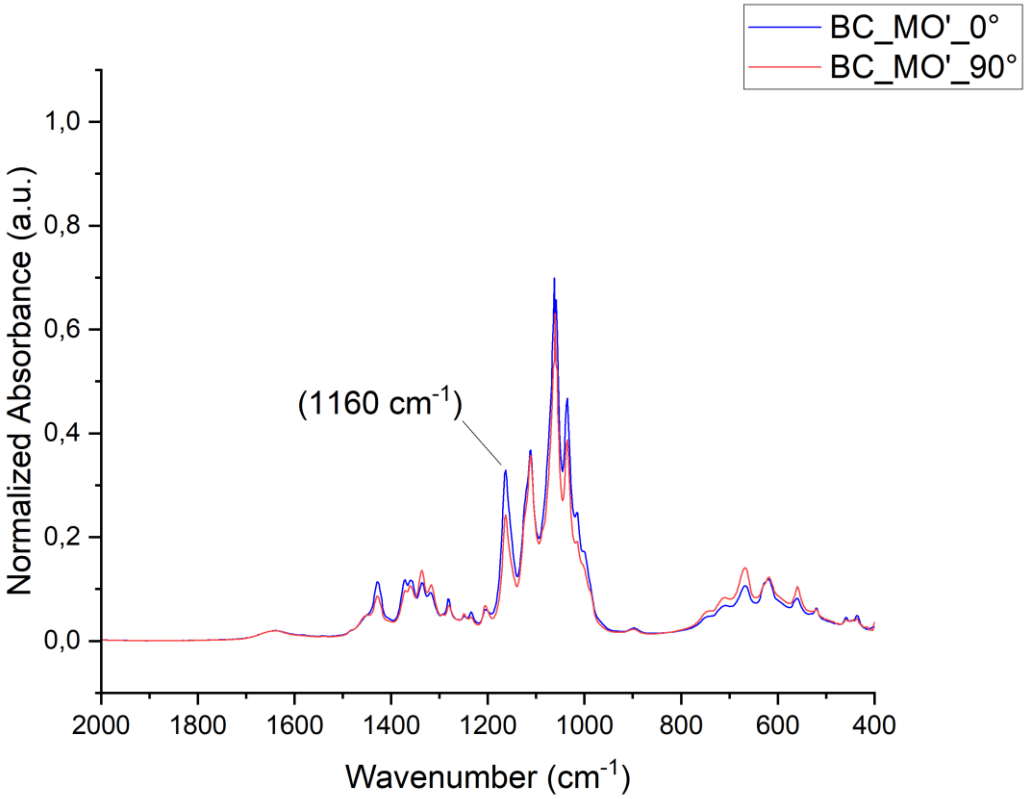

Figure 5.11: pFTIR of BC restricted dried with abrasive between the “claws” in the parallel (blue) and perpendicular (red) of the constrained direction.

5.4 Scanning electron microscopy (SEM)

The surface and cryo-fractured cross-sections of the different BC films were characterized morphologically by SEM. To enable proper comparison, the samples were carefully positioned longitudinally on the stubs (Figure 5.12). The

stubs, in turn, were also positioned carefully so that it was possible to see the marking line of the carbon tape to make this process as reliable as possible if the direction of the microfibrils that are observed were oriented in the longitudinal direction, which was the direction of the pre-stretching and restriction. From the obtained micrographs, the OrientationJ plugin, which is a series of ImageJ software plugins for analyzing directional images, was used. This resource is widely used in other literature to quantify fiber alignment and other studies that consider the orientation of a material (Fee et al., 2016; Rezakhaniha et al., 2012; Sharabi et al., 2015)A color map (Figure 5.13) can be seen from the obtained and treated micrographs, showing the relationship between the local angular direction and a given color.

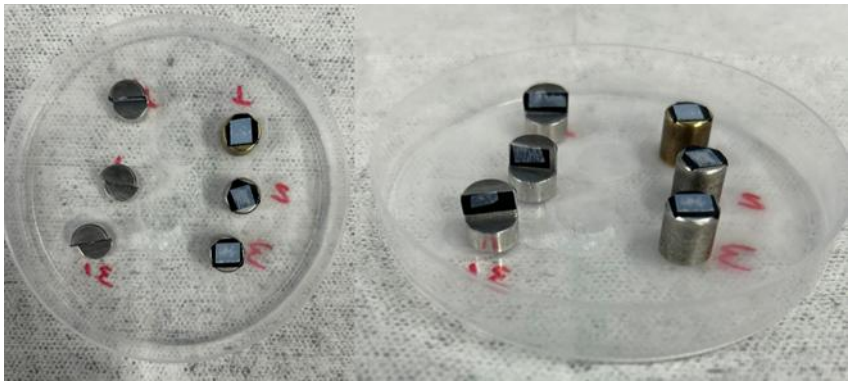

Figure 5.12: Stubs topped with the bacterial cellulose samples.

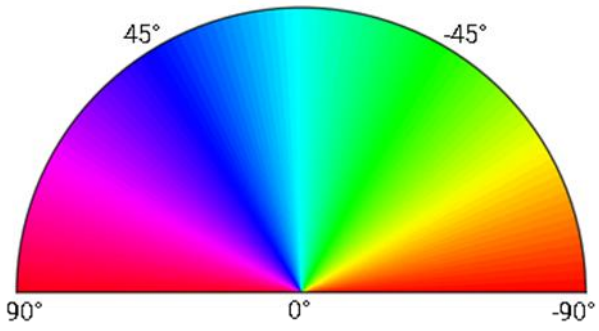

Figure 5.13: Color map following the Hue, Saturation, Value (HSV) color model.

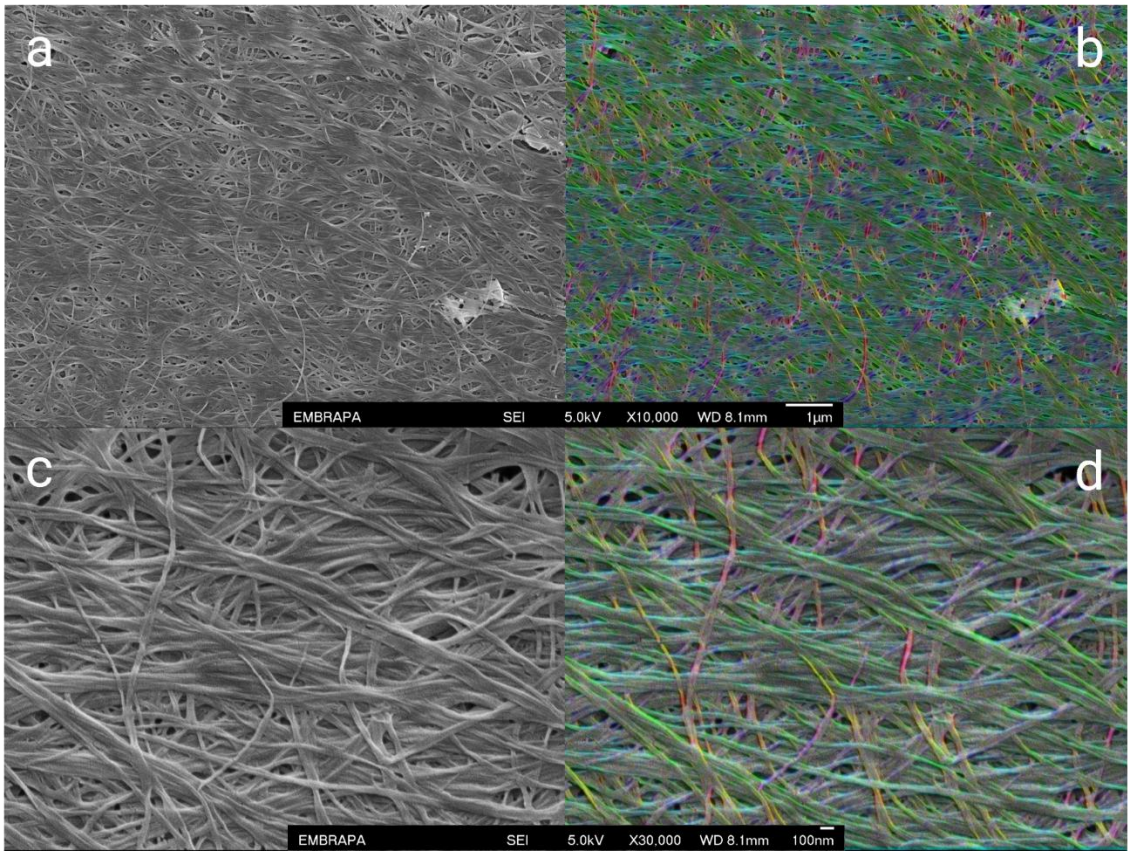

Figure 5.14: SEM of “freely” dried BC at two different scales represented by the letters (a and c) and the respective images generated by the OrientationJ plugin (b and d), where each color represents an orientation angle.

Figure 5.14 evidence that BC has a preferential direction distribution of its microfibrils around 20° since the greenish color is predominant in Figures 5.14b and 5.14d. In contrast, Figures 5.15 and 5.16 show a change in this distribution, where BC films that have been dried restrictively under pre-stretching to cause orientation to have a predominantly red and pink coloration, which means that the most abundant local preferential direction is around 90°, which would be precisely the axial direction used to dry the film.

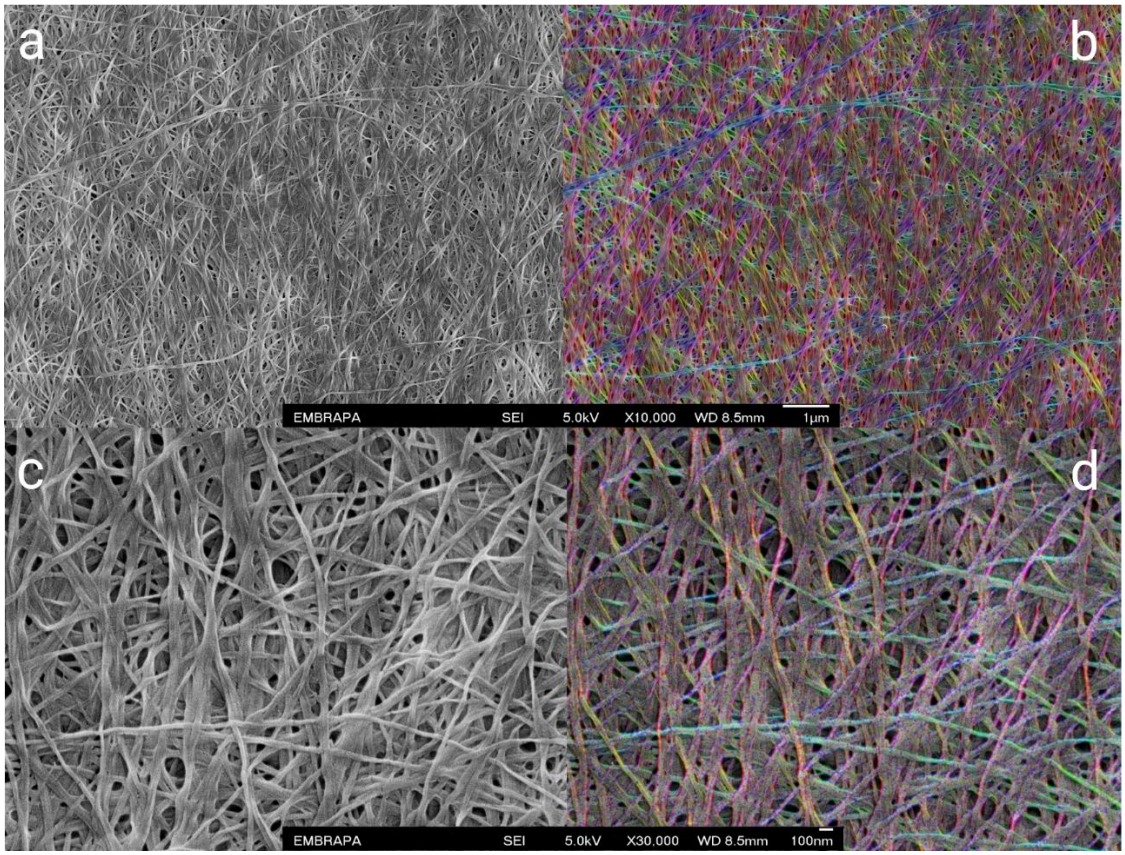

Figure 5.15: SEM of restricted dried BC with pre-stretching but without the abrasive at two different scales represented by the letters (a and c) and the respective images generated by the OrientationJ plugin (b and d), where each color represents an orientation angle.

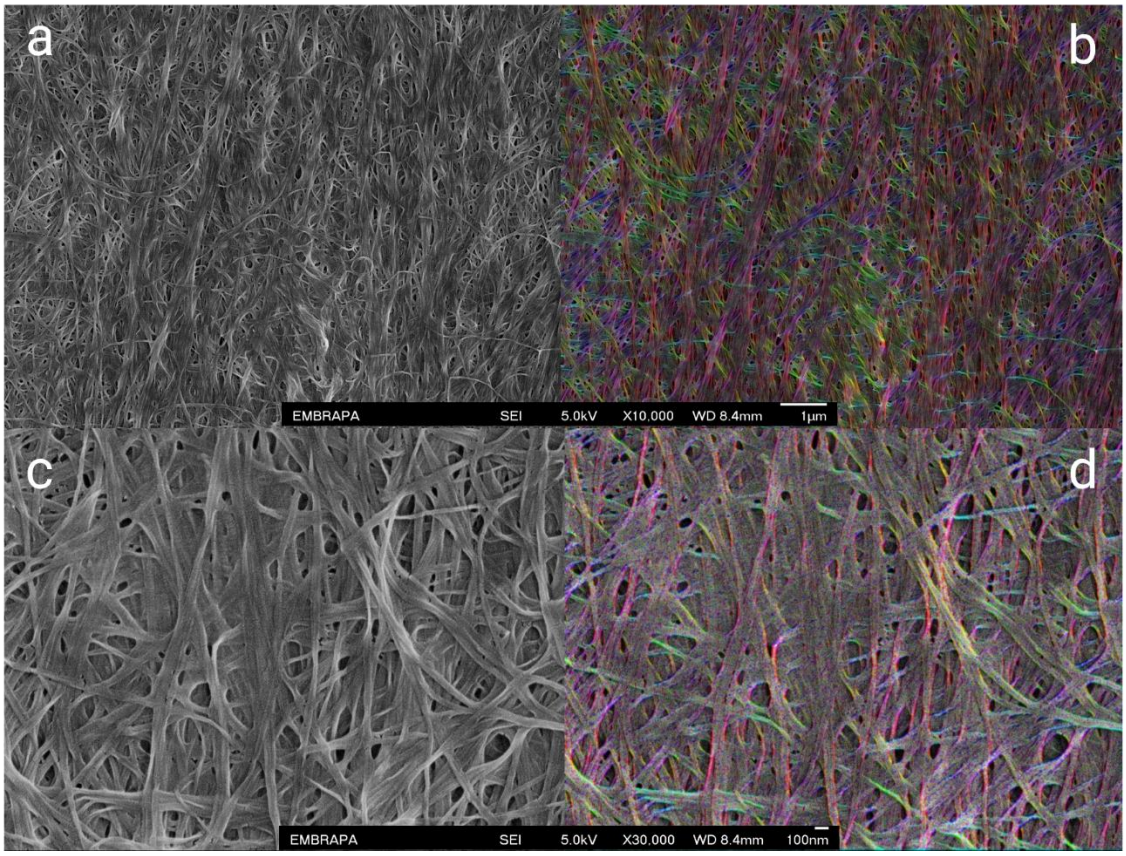

Figure 5.16: SEM of BC restricted dried with abrasive between the “claws” at two different scales represented by the letters (a and c) and the respective images generated in the same scale by the OrientationJ plugin (b and d), where each color represents an orientation angle.

Figure 5.17 shows the relationship between the distribution of microfibril orientation and the angle at which they are oriented. The change in orientation from ordinary BC to oriented BC can be seen more clearly in this graph, as the maximum peaks of the curves are found, as previously mentioned, between 20° for the ordinary BC curve and 90° for the mono-oriented BC films. This highlights the wider distribution of orientation around the axial direction in the BC film bearing the greatest birefringence, corroborating the previous tests.

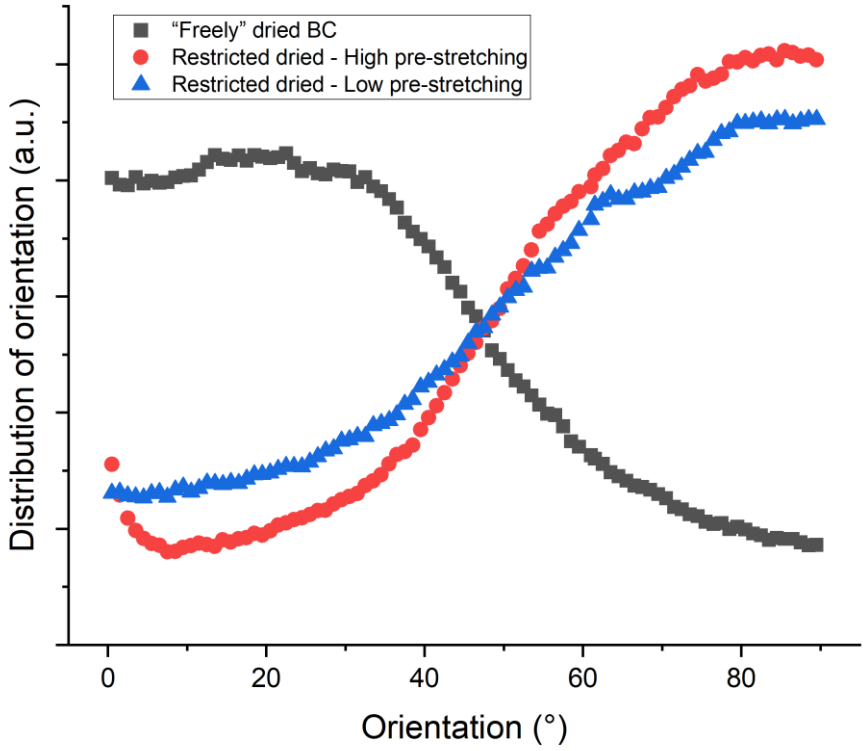

Figure 5.17: Distribution graph from orientation angle and angular density distributions of "freely" dried BC (black); BC with pre-stretching but without the abrasive(blue); BC restricted dried with abrasive between the "claws" (red).

As for the cryo-fracture micrographs (Figure 5.18), the BC film has a veneer structure, just as in the literature (GROMOVYKH *et al.*, 2020; WU *et al.*, 2023). When it goes through the drying-induced orientation process, there is a greater density of microfibrils that follow an order in the fracture region, while for ordinary BC, there is a presence of microfibrils that are more scattered "randomly", which suggests that these strong interconnections of the microfibrils end up generating greater tensile strengths and moduli in the oriented direction.

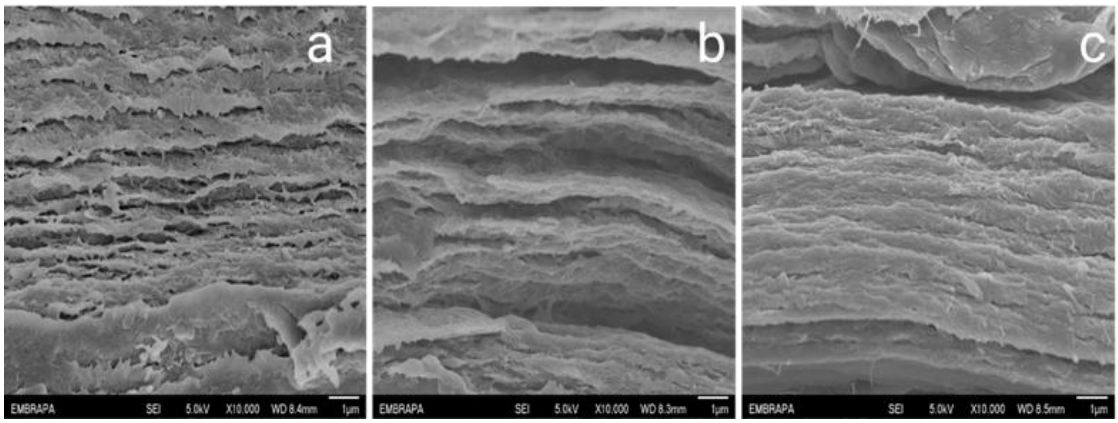

Figure 5.18: Cryofracture surface of SEM in BC films. a) "freely" dried BC; b) BC with pre-stretching but without the abrasive and c) BC restricted dried with abrasive between the "claws".

5.5 X-ray diffraction (XRD)

X-ray diffraction was carried out to confirm the influence of the restrict drying in the crystalline structure of cellulose. The crystallinity index (CI) of the samples, was calculated according with the Ruland method (Equation 5.1),

$$Crystallinity\ (\%) = \left(\frac{Acrystalline}{Atotal}\right) \times 100 \qquad \text{(Equation 5.1)}$$

$A_{crystalline}$ is the sum of the area of all crystalline peaks and A_{total} is the sum of the crystalline area and the amorphous area under the curve in the XRD pattern. The calculated percentages of crystallinity for the BC samples can be seen in the Table 2 below

Table 5.6: Apparent crystallinity index (CI) at the center and edge regions of bacterial cellulose (BC) films dried under free and restricted conditions, the latter submitted to low- and high pre-stretching levels (BC_MO and BC_MO').

BC Sample	Crystallinity Index (%) (Center)	Crystallinity Index (%) (Edge)
BC	74.7	73.6
BC_MO	78.3	74.9
BC_MO'	78.7	76.5

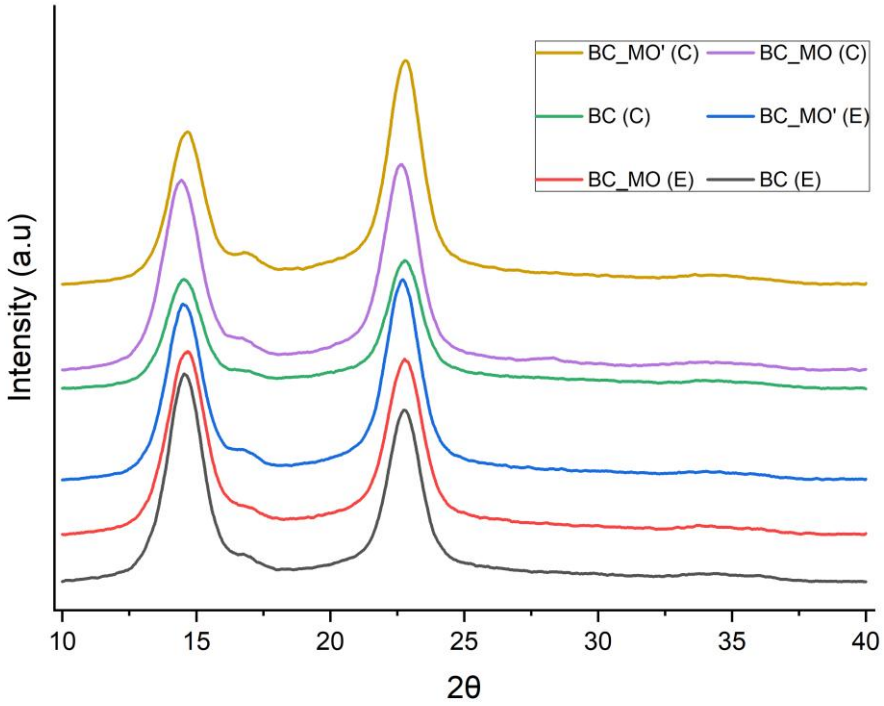

Figure 5.19: X-ray diffractogram of freely" dried BC (BC); Restricted Dried BC but without the abrasive (BC_MO) and restricted dried BC with abrasive between the "claws" (BC_MO'). Two sections were analyzed the center (C), the edge (E) of the samples.

From the XRD patterns, we can see that in Figure 5.19 there is three common crystalline peaks at around 14.5°, 16.7°, and 22.7°, corresponding to the (101), ($10\bar{1}$), and (002) planes of bacterial cellulose (ABRAL et al., 2021; FOSTER et al., 2018; ZENG; LAROMAINE; ROIG, 2014). The results show no significant difference in crystallinity. However, the calculated percentage for these samples shows that a slight increased CI is reached for the BC that was pre-stretched and dried by the restrict protocols. This apparent increase may be explained by the alignment of BC microfibrils, as demonstrated in previous tests. Such alignment can promote a more tightly packed structure with greater microfibril stacking, leading to a reduction in pore volume and, consequently, an increase in crystallinity (Prathapan et al., 2020b).

5.6 Dynamic Mechanical Analysis (DMA)

The mechanical properties of the BC films were analyzed using the DMA (Figure 5.20). First, the films were tested in two main directions: parallel (0°) and transverse (90°) to the direction of orientation. According to Table 5.7 and Figure 5.20, preferential orientation increased Young's modulus and tensile strength in the parallel direction, while the samples became less stiff, though more resistant, in the transverse direction. As expected, freely dried BC was mechanically isotropic. Elongation at break was only mildly affected. As BC consists of a continuous network of fibers with cross-linked nodes and absence of fully isolated fibers, its response to stress is associated with cellulose-cellulose slippage, breaking of covalent bonds, and the bending of fibers. Therefore, the observed anisotropy in aligned samples results from the energy required to overcome secondary (e.g., hydrogen bonding, van der Waals) interactions for partial slippage of fibers when stretching films in MD. However, slippage and secondary interactions will have marginal effect compared to fibers bending in out of alignment planes (Luotonen et al., 2022). Therefore, in TD, the response to stress can principally be associated with fiber bending and loose fibers slippage in the stress direction.

Table 5.7: The average tensile strength, elongation at break and Young's modulus calculated using the acquired Stress x Strain curves of the "freely" dried BC, BC restricted dried (BC_MO) and with abrasive between the "claws" (BC MO') in the perpendicular direction (90°) of the restrain and parallel (0°).

Material	Tensile strength (MPa)		Elongation at break (%)		Young's modulus (GPa)	
	∥ (0°)	⊥ (90°)	∥ (0°)	⊥ (90°)	∥ (0°)	⊥ (90°)
BC	59.1 ± 3.4	63.8 ± 7.0	1.0 ± 0.1	1.3 ± 0.13	7.6 ± 0.1	7.7 ± 1.3
BC_MO	122.2 ± 12.8	93.4 ± 3.7	1.4 ± 0.1	3.9 ± 0.4	17.2 ± 0.3	5.4 ± 0.1
BC_MO'	123.8 ± 11.0	111.36 ± 2.2	1.0 ± 0.07	4.6 ± 0.6	21.2 ± 0.2	5.1 ± 0.1

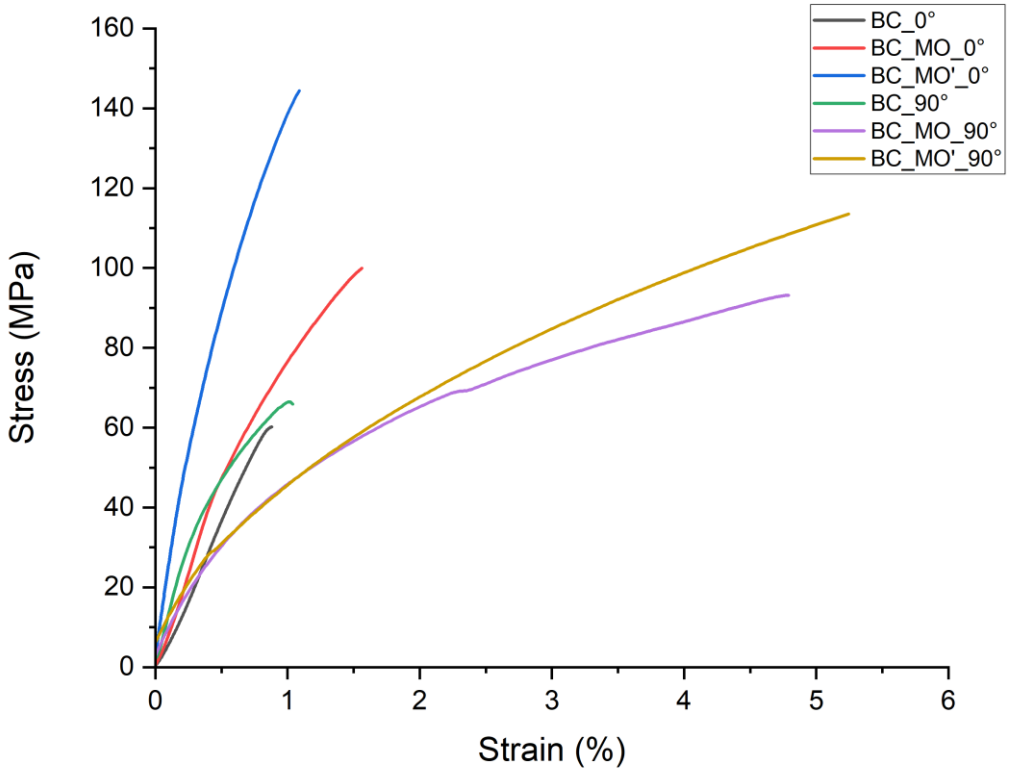

Figure 5.20: Stress x Strain curves of dried BC on different drying procedures and directions used on the test. The angles are parallel (0°) and transverse (90°) to the direction of orientation.

6 CONCLUSION

This work evaluates the relationship between optical response, chemical as well as diffractive fingers prints, and anisotropy of mechanical response for uniaxially oriented fibers as obtained from axial restriction during drying. The monodirectional BC films exhibit enhanced interfibrillar interactions, reduced porosity, an apparent increase in CI, and pronounced optical anisotropy. The extent of stretching applied prior to drying plays a decisive role in controlling the degree of fibril orientation, with higher pre-stretch levels (BC_MO and BC_MO') leading to greater alignment during consolidation. As a direct consequence, the restricted dried films display clear mechanical anisotropy, with distinct stiffness, strength, and deformation behavior along directions parallel and perpendicular to the orientation axis, in contrast to the isotropic response of freely dried BC. The study elucidates the structure/property relationships in the obtained BC with long-range ordered fibers, as obtained from a simple, low-cost, and solvent-free alignment approach. While further optimization is required to improve drying kinetics, fixation strategies, and scalability for industrial implementation, the results highlight the strong potential of controlled drying as a versatile tool to tailor the structural, optical, and mechanical performance of BC films for applications in composites, sensors, and smart or functional bio-based devices.

7 FUTURE WORKS

- Optimize the amount of orientation introduced from other drying parameters, such as different relative humidity, drying environment temperatures, and others;
- Optimize the drying frame regarding size and force on the restriction so that greater pre-stretch can be introduced into the film without slipping;
- Trying to produce a unique augmented birefringence BC film;
- Investigate more about the changes in crystalline index of BC during the drying process and employ small-angle X-ray scattering (SAXS) to determine the Herman’s orientation parameters;
- Use Polarized Light Optical Microscopy to calculate the average birefringence of the BC microfibrils;

8 REFERENCES

Abral, H., Chairani, M. K., Rizki, M. D., Mahardika, M., Handayani, D., Sugiarti, E., Muslimin, A. N., Sapuan, S. M., & Ilyas, R. A. (2021). Characterization of compressed bacterial cellulose nanopaper film after exposure to dry and humid conditions. *Journal of Materials Research and Technology*, *11*, 896–904. https://doi.org/https://doi.org/10.1016/j.jmrt.2021.01.057

Ahmed, J., Gultekinoglu, M., & Edirisinghe, M. (2020). Bacterial cellulose micro-nano fibres for wound healing applications. *Biotechnology Advances*, *41*, 107549. https://doi.org/https://doi.org/10.1016/j.biotechadv.2020.107549

Alcock, B., Cabrera, N. O., Barkoula, N. M., & Peijs, T. (2009). The effect of processing conditions on the mechanical properties and thermal stability of highly oriented PP tapes. *European Polymer Journal*, *45*(10), 2878–2894. https://doi.org/https://doi.org/10.1016/j.eurpolymj.2009.06.025

Amorim, L. F. A., Mouro, C., Riool, M., & Gouveia, I. C. (2022). Antimicrobial Food Packaging Based on Prodigiosin-Incorporated Double-Layered Bacterial Cellulose and Chitosan Composites. *Polymers*, *14*(2). https://doi.org/10.3390/polym14020315

Andree, V., Niopek, D., Müller, C., Eiselt, J.-P., Foh, N., Rzany, A., & Hensel, B. (2021). Influence of drying methods on the physical properties of bacterial nanocellulose. *Materials Research Express*, *8*(2), 025402. https://doi.org/10.1088/2053-1591/abe016

Arikibe, J. E., Lata, R., Kuboyama, K., Ougizawa, T., & Rohindra, D. (2019). pH-Responsive Studies of Bacterial Cellulose /Chitosan Hydrogels Crosslinked with Genipin: Swelling and Drug Release Behaviour. *ChemistrySelect*, *4*(34), 9915–9926. https://doi.org/https://doi.org/10.1002/slct.201902290

Atykyan, N., Revin, V., & Shutova, V. (2020). Raman and FT-IR Spectroscopy investigation the cellulose structural differences from bacteria Gluconacetobacter sucrofermentans during the different regimes of cultivation on a molasses media. *AMB Express*, *10*(1), 84. https://doi.org/10.1186/s13568-020-01020-8

Bartczak, Z., Morawiec, J., & Galeski, A. (2002). Deformation of high-density polyethylene produced by rolling with side constraints. II. Mechanical

properties of oriented bars. *Journal of Applied Polymer Science*, *86*(6), 1405–1412. https://doi.org/https://doi.org/10.1002/app.11286

Belbachir, K., Lecomte, S., Ta, H.-P., Petibois, C., & Desbat, B. (2011). Orientation of molecular groups of fibers in nonoriented samples determined by polarized ATR-FTIR spectroscopy. *Analytical and Bioanalytical Chemistry*, *401*(10), 3263–3268. https://doi.org/10.1007/s00216-011-5418-0

Binder, S., Stanzel, B. V, Krebs, I., & Glittenberg, C. (2007). Transplantation of the RPE in AMD. *Progress in Retinal and Eye Research*, *26*(5), 516–554. https://doi.org/https://doi.org/10.1016/j.preteyeres.2007.02.002

Breijaert, T. C., Fontes, M., Fernandes, P. de A., Barud, H. da S., Ribeiro, S. J. L., & Seisenbaeva, G. A. (2025). Functionalization of bacterial nanocellulose-based wound dressing for increased drug retention. *Carbohydrate Polymer Technologies and Applications*, *10*, 100756. https://doi.org/https://doi.org/10.1016/j.carpta.2025.100756

Brown, A. J. (1886). XLIII.—On an acetic ferment which forms cellulose. *Journal of the Chemical Society, Transactions*, *49*(0), 432–439. https://doi.org/10.1039/CT8864900432

Brown Jr., R. M. (2004). Cellulose structure and biosynthesis: What is in store for the 21st century? *Journal of Polymer Science Part A: Polymer Chemistry*, *42*(3), 487–495. https://doi.org/https://doi.org/10.1002/pola.10877

Cacicedo, M. L., Castro, M. C., Servetas, I., Bosnea, L., Boura, K., Tsafrakidou, P., Dima, A., Terpou, A., Koutinas, A., & Castro, G. R. (2016). Progress in bacterial cellulose matrices for biotechnological applications. *Bioresource Technology*, *213*, 172–180. https://doi.org/https://doi.org/10.1016/j.biortech.2016.02.071

Castro, C., Zuluaga, R., Álvarez, C., Putaux, J.-L., Caro, G., Rojas, O. J., Mondragon, I., & Gañán, P. (2012). Bacterial cellulose produced by a new acid-resistant strain of Gluconacetobacter genus. *Carbohydrate Polymers*, *89*(4), 1033–1037. https://doi.org/https://doi.org/10.1016/j.carbpol.2012.03.045

Cheng, K.-C., Catchmark, J. M., & Demirci, A. (2011). Effects of CMC Addition on Bacterial Cellulose Production in a Biofilm Reactor and Its Paper Sheets

Analysis. *Biomacromolecules*, *12*(3), 730–736. https://doi.org/10.1021/bm101363t

Choi, S. M., Rao, K. M., Zo, S. M., Shin, E. J., & Han, S. S. (2022). Bacterial Cellulose and Its Applications. *Polymers*, *14*(6). https://doi.org/10.3390/polym14061080

Costa, A. F. S., Almeida, F. C. G., Vinhas, G. M., & Sarubbo, L. A. (2017). Production of Bacterial Cellulose by Gluconacetobacter hansenii Using Corn Steep Liquor As Nutrient Sources. *Frontiers in Microbiology*, *8*. https://www.frontiersin.org/articles/10.3389/fmicb.2017.02027

Czaja, W., Romanovicz, D., & Brown, R. malcolm. (2004). Structural investigations of microbial cellulose produced in stationary and agitated culture. *Cellulose*, *11*(3), 403–411. https://doi.org/10.1023/B:CELL.0000046412.11983.61

Dhar, P., Etula, J., & Bankar, S. B. (2019). In Situ Bioprocessing of Bacterial Cellulose with Graphene: Percolation Network Formation, Kinetic Analysis with Physicochemical and Structural Properties Assessment. *ACS Applied Bio Materials*, *2*(9), 4052–4066. https://doi.org/10.1021/acsabm.9b00581

Ek Monica, Gellerstedt Göran, & Henriksson Gunna. (2009). *Volume 1 Wood Chemistry and Wood Biotechnology*. De Gruyter. https://doi.org/doi:10.1515/9783110213409

Fee, T., Downs, C., Eberhardt, A., Zhou, Y., & Berry, J. (2016). Image-based quantification of fiber alignment within electrospun tissue engineering scaffolds is related to mechanical anisotropy. *Journal of Biomedical Materials Research Part A*, *104*(7), 1680–1686. https://doi.org/https://doi.org/10.1002/jbm.a.35697

Fink, H.-P., Purz, H. J., Bohn, A., & Kunze, J. (1997). Investigation of the supramolecular structure of never dried bacterial cellulose. *Macromolecular Symposia*, *120*(1), 207–217. https://doi.org/https://doi.org/10.1002/masy.19971200121

Foster, E. J., Moon, R. J., Agarwal, U. P., Bortner, M. J., Bras, J., Camarero-Espinosa, S., Chan, K. J., Clift, M. J. D., Cranston, E. D., Eichhorn, S. J., Fox, D. M., Hamad, W. Y., Heux, L., Jean, B., Korey, M., Nieh, W., Ong, K.

J., Reid, M. S., Renneckar, S., … Youngblood, J. (2018). Current characterization methods for cellulose nanomaterials. *Chemical Society Reviews*, *47*(8), 2609–2679. https://doi.org/10.1039/C6CS00895J

Gandini, A., & Lacerda, T. M. (2015). From monomers to polymers from renewable resources: Recent advances. *Progress in Polymer Science*, *48*, 1–39. https://doi.org/https://doi.org/10.1016/j.progpolymsci.2014.11.002

Gao, H., Cao, W., He, J., & Bai, Y. (2021). Highly transparent biaxially oriented poly(ester amide) film with improved gas barrier properties and good mechanical strength. *European Polymer Journal*, *156*, 110620. https://doi.org/https://doi.org/10.1016/j.eurpolymj.2021.110620

Gatenholm, P., & Klemm, D. (2010). Bacterial Nanocellulose as a Renewable Material for Biomedical Applications. *MRS Bulletin*, *35*(3), 208–213. https://doi.org/10.1557/mrs2010.653

Gibson, A. G., & Ward, I. M. (1980). The manufacture of ultra-high modulus polyethylenes by drawing through a conical die. *Journal of Materials Science*, *15*(4), 979–986. https://doi.org/10.1007/BF00552111

Guo, Y., Zhang, X., Hao, W., Xie, Y., Chen, L., Li, Z., Zhu, B., & Feng, X. (2018). Nano-bacterial cellulose/soy protein isolate complex gel as fat substitutes in ice cream model. *Carbohydrate Polymers*, *198*, 620–630. https://doi.org/https://doi.org/10.1016/j.carbpol.2018.06.078

He, X., Meng, H., Song, H., Deng, S., He, T., Wang, S., Wei, D., & Zhang, Z. (2020). Novel bacterial cellulose membrane biosynthesized by a new and highly efficient producer Komagataeibacter rhaeticus TJPU03. *Carbohydrate Research*, *493*, 108030. https://doi.org/https://doi.org/10.1016/j.carres.2020.108030

Hecht, E. (2002). *Optics, 5e*. Pearson Education India.

Hernane Barud, S. (2010). *Materiais multifuncionais baseados em celulose bacteriana*. http://hdl.handle.net/11449/105766

Hong, F., Guo, X., Zhang, S., Han, S., Yang, G., & Jönsson, L. J. (2012). Bacterial cellulose production from cotton-based waste textiles: Enzymatic saccharification enhanced by ionic liquid pretreatment. *Bioresource*

Technology, *104*, 503–508. https://doi.org/https://doi.org/10.1016/j.biortech.2011.11.028

Hussain, Z., Sajjad, W., Khan, T., & Wahid, F. (2019). Production of bacterial cellulose from industrial wastes: a review. *Cellulose*, *26*(5), 2895–2911. https://doi.org/10.1007/s10570-019-02307-1

Illa, M. P., Sharma, C. S., & Khandelwal, M. (2019). Tuning the physiochemical properties of bacterial cellulose: effect of drying conditions. *Journal of Materials Science*, *54*(18), 12024–12035. https://doi.org/10.1007/s10853-019-03737-9

Inoue, T. (2021). Strain-Induced Birefringence of Amorphous Polymers and Molecular Design of Optical Polymers. *ACS Applied Polymer Materials*, *3*(5), 2264–2273. https://doi.org/10.1021/acsapm.1c00149

Islam, M. U., Ullah, M. W., Khan, S., Shah, N., & Park, J. K. (2017). Strategies for cost-effective and enhanced production of bacterial cellulose. *International Journal of Biological Macromolecules*, *102*, 1166–1173. https://doi.org/https://doi.org/10.1016/j.ijbiomac.2017.04.110

Jiang, W., Jiang, Z., Zhu, M., & Fan, X. (2022). Oriented bacterial cellulose for achieving high carbon yield through pre-stretching. *Cellulose*, *29*(8), 4323–4333. https://doi.org/10.1007/s10570-022-04559-w

Jin, Z., Yang, Y., Siregar, M. I., Mu, Z., Islam, S. M. A., Zhao, Q., Wang, D., Zhang, F., Yang, X., & Song, L. (2024). Seismic anisotropy and upper mantle dynamics in Alaska: A review of shear wave splitting analyses. *Earthquake Research Advances*, 100289. https://doi.org/https://doi.org/10.1016/j.eqrea.2024.100289

Kafle, K., Park, Y. B., Lee, C. M., Stapleton, J. J., Kiemle, S. N., Cosgrove, D. J., & Kim, S. H. (2017). Effects of mechanical stretching on average orientation of cellulose and pectin in onion epidermis cell wall: A polarized FT-IR study. *Cellulose*, *24*(8), 3145–3154. https://doi.org/10.1007/s10570-017-1337-3

Kakade, M. V, Givens, S., Gardner, K., Lee, K. H., Chase, D. B., & Rabolt, J. F. (2007). Electric Field Induced Orientation of Polymer Chains in Macroscopically Aligned Electrospun Polymer Nanofibers. *Journal of the*

American Chemical Society, *129*(10), 2777–2782. https://doi.org/10.1021/ja065043f

Katoh, K., Hammar, K., Smith, P. J. S., & Oldenbourg, R. (1999). Birefringence Imaging Directly Reveals Architectural Dynamics of Filamentous Actin in Living Growth Cones. *Molecular Biology of the Cell*, *10*(1), 197–210. https://doi.org/10.1091/mbc.10.1.197

Klemm, D., Schumann, D., Kramer, F., Heßler, N., Hornung, M., Schmauder, H.-P., & Marsch, S. (2006). Nanocelluloses as Innovative Polymers in Research and Application. In D. Klemm (Ed.), *Polysaccharides II* (pp. 49–96). Springer Berlin Heidelberg. https://doi.org/10.1007/12_097

Lahiri, D., Nag, M., Dutta, B., Dey, A., Sarkar, T., Pati, S., Edinur, H. A., Abdul Kari, Z., Mohd Noor, N. H., & Ray, R. R. (2021). Bacterial Cellulose: Production, Characterization, and Application as Antimicrobial Agent. *International Journal of Molecular Sciences*, *22*(23). https://doi.org/10.3390/ijms222312984

Lee, S. E., & Park, Y. S. (2017). The role of bacterial cellulose in artificial blood vessels. *Molecular & Cellular Toxicology*, *13*(3), 257–261. https://doi.org/10.1007/s13273-017-0028-3

Legnani, C., Barud, H. S., Caiut, J. M. A., Calil, V. L., Maciel, I. O., Quirino, W. G., Ribeiro, S. J. L., & Cremona, M. (2019). Transparent bacterial cellulose nanocomposites used as substrate for organic light-emitting diodes. *Journal of Materials Science: Materials in Electronics*, *30*(18), 16718–16723. https://doi.org/10.1007/s10854-019-00979-w

Lepers, J.-C., Favis, B. D., & Kent, S. L. (1999). - Study of the Morphology and the Tensile Mechanical Properties of Biaxially Oriented PET/PP Blends. In B. Pourdeyhimi (Ed.), *Imaging and Image Analysis Applications for Plastics* (pp. 119–126). William Andrew Publishing. https://doi.org/https://doi.org/10.1016/B978-188420781-5.50016-4

Li, T., Chen, C., Brozena, A. H., Zhu, J. Y., Xu, L., Driemeier, C., Dai, J., Rojas, O. J., Isogai, A., Wågberg, L., & Hu, L. (2021). Developing fibrillated cellulose as a sustainable technological material. *Nature*, *590*(7844), 47–56. https://doi.org/10.1038/s41586-020-03167-7

Lima, L. R., Santos, D. B., Santos, M. V., Barud, H. S., Henrique, M. A., Pasquini, D., Pecoraro, E., & Ribeiro, S. J. L. (2015). CELLULOSE NANOCRYSTALS FROM BACTERIAL CELLULOSE. *Química Nova*, *38*, 1140–1147. https://doi.org/10.5935/0100-4042.20150131

Lin, D., Liu, Z., Shen, R., Chen, S., & Yang, X. (2020). Bacterial cellulose in food industry: Current research and future prospects. *International Journal of Biological Macromolecules*, *158*, 1007–1019. https://doi.org/https://doi.org/10.1016/j.ijbiomac.2020.04.230

Luotonen, O. I. V, Greca, L. G., Nyström, G., Guo, J., Richardson, J. J., Rojas, O. J., & Tardy, B. L. (2022). Benchmarking supramolecular adhesive behavior of nanocelluloses, cellulose derivatives and proteins. *Carbohydrate Polymers*, *292*, 119681. https://doi.org/https://doi.org/10.1016/j.carbpol.2022.119681

Maia, G. T. da S., Albuquerque, A. V. de, Martins Filho, E. D., Lira Neto, F. T. de, Souza, V. S. B. de, Silva, A. A. da, Lira, M. M. de M., & Lima, S. V. C. (2018). Bacterial cellulose to reinforce urethrovesical anastomosis. A translational study. *Acta Cirurgica Brasileira*, *33*(8), 673–683. https://doi.org/10.1590/s0102-865020180080000003

Marchetti, L., Muzzio, B., Cerrutti, P., Andrés, S. C., & Califano, A. N. (2017). Bacterial nanocellulose as novel additive in low-lipid low-sodium meat sausages. Effect on quality and stability. *Food Structure*, *14*, 52–59. https://doi.org/https://doi.org/10.1016/j.foostr.2017.06.004

Marestoni, L. D., Barud, H. da S., Gomes, R. J., Catarino, R. P. F., Hata, N. N. Y., Ressutte, J. B., & Spinosa, W. A. (2020). Commercial and potential applications of bacterial cellulose in Brazil: ten years review. *Polímeros*, *30*(4), e2020047. https://doi.org/10.1590/0104-1428.09420

Mbituyimana, B., Liu, L., Ye, W., Ode Boni, B. O., Zhang, K., Chen, J., Thomas, S., Vasilievich, R. V., Shi, Z., & Yang, G. (2021). Bacterial cellulose-based composites for biomedical and cosmetic applications: Research progress and existing products. *Carbohydrate Polymers*, *273*, 118565. https://doi.org/https://doi.org/10.1016/j.carbpol.2021.118565

Medhat, M., El-Zaiat, S. Y., Ramadan, H., & Abdelghaffar, M. (2017). Effect of thermal annealing on the linear birefringence of polystyrene, polypropylene and cellulose acetate polymers. *Optik*, *131*, 490–496. https://doi.org/https://doi.org/10.1016/j.ijleo.2016.11.044

Medronho, B., Romano, A., Miguel, M. G., Stigsson, L., & Lindman, B. (2012). Rationalizing cellulose (in)solubility: reviewing basic physicochemical aspects and role of hydrophobic interactions. *Cellulose*, *19*(3), 581–587. https://doi.org/10.1007/s10570-011-9644-6

Mredha, Md. T. I., Guo, Y. Z., Nonoyama, T., Nakajima, T., Kurokawa, T., & Gong, J. P. (2018). A Facile Method to Fabricate Anisotropic Hydrogels with Perfectly Aligned Hierarchical Fibrous Structures. *Advanced Materials*, *30*(9), 1704937. https://doi.org/https://doi.org/10.1002/adma.201704937

Nakayama, K., & Kanetsuna, H. (1975). Hydrostatic extrusion of solid polymers. *Journal of Materials Science*, *10*(7), 1105–1118. https://doi.org/10.1007/BF00541391

Naomi, R., Bt Hj Idrus, R., & Fauzi, M. B. (2020). Plant- vs. Bacterial-Derived Cellulose for Wound Healing: A Review. *International Journal of Environmental Research and Public Health*, *17*(18). https://doi.org/10.3390/ijerph17186803

Navya, P. V, Gayathri, V., Samanta, D., & Sampath, S. (2022). Bacterial cellulose: A promising biopolymer with interesting properties and applications. *International Journal of Biological Macromolecules*, *220*, 435–461. https://doi.org/https://doi.org/10.1016/j.ijbiomac.2022.08.056

Nechita, P., Mirela, R., & Ciolacu, F. (2021). Xylan Hemicellulose: A Renewable Material with Potential Properties for Food Packaging Applications. *Sustainability*, *13*(24). https://doi.org/10.3390/su132413504

Pandey, M., Mohamad, N., & Amin, M. C. I. M. (2014). Bacterial Cellulose/Acrylamide pH-Sensitive Smart Hydrogel: Development, Characterization, and Toxicity Studies in ICR Mice Model. *Molecular Pharmaceutics*, *11*(10), 3596–3608. https://doi.org/10.1021/mp500337r

Postolache, M., Dimitriu, D. G., Nechifor, C. D., Condurache Bota, S., Closca, V., & Dorohoi, D. O. (2022). Birefringence of Thin Uniaxial Polymer Films

Estimated Using the Light Polarization Ellipse. *Polymers*, *14*(5). https://doi.org/10.3390/polym14051063

Prathapan, R., Ghosh, A. K., Knapp, A., Vijayakumar, A., Bogari, N. N. J., Abraham, B. D., Al-Ghabkari, A., Fery, A., & Hu, J. (2020a). In Situ Alignment of Bacterial Cellulose Using Wrinkling. *ACS Applied Bio Materials*, *3*(11), 7898–7907. https://doi.org/10.1021/acsabm.0c01030

Prathapan, R., Ghosh, A. K., Knapp, A., Vijayakumar, A., Bogari, N. N. J., Abraham, B. D., Al-Ghabkari, A., Fery, A., & Hu, J. (2020b). In Situ Alignment of Bacterial Cellulose Using Wrinkling. *ACS Applied Bio Materials*, *3*(11), 7898–7907. https://doi.org/10.1021/acsabm.0c01030

Raiszadeh-Jahromi, Y., Rezazadeh-Bari, M., Almasi, H., & Amiri, S. (2020). Optimization of bacterial cellulose production by Komagataeibacter xylinus PTCC 1734 in a low-cost medium using optimal combined design. *Journal of Food Science and Technology*, *57*(7), 2524–2533. https://doi.org/10.1007/s13197-020-04289-6

Rezakhaniha, R., Agianniotis, A., Schrauwen, J. T. C., Griffa, A., Sage, D., Bouten, C. V. C., van de Vosse, F. N., Unser, M., & Stergiopulos, N. (2012). Experimental investigation of collagen waviness and orientation in the arterial adventitia using confocal laser scanning microscopy. *Biomechanics and Modeling in Mechanobiology*, *11*(3), 461–473. https://doi.org/10.1007/s10237-011-0325-z

Ruland, W. (1961). X-ray determination of crystallinity and diffuse disorder scattering. *Acta Crystallographica*, *14*(11), 1180–1185. https://doi.org/https://doi.org/10.1107/S0365110X61003429

Sharabi, M., Benayahu, D., Benayahu, Y., Isaacs, J., & Haj-Ali, R. (2015). Laminated collagen-fiber bio-composites for soft-tissue bio-mimetics. *Composites Science and Technology*, *117*, 268–276. https://doi.org/https://doi.org/10.1016/j.compscitech.2015.06.024

Shavyrkina, N. A., Skiba, E. A., Kazantseva, A. E., Gladysheva, E. K., Budaeva, V. V, Bychin, N. V, Gismatulina, Y. A., Kashcheyeva, E. I., Mironova, G. F., Korchagina, A. A., Pavlov, I. N., & Sakovich, G. V. (2021). Static Culture

Combined with Aeration in Biosynthesis of Bacterial Cellulose. *Polymers*, *13*(23). https://doi.org/10.3390/polym13234241

Shi, Z., Zhang, Y., Phillips, G. O., & Yang, G. (2014). Utilization of bacterial cellulose in food. *Food Hydrocolloids*, *35*, 539–545. https://doi.org/https://doi.org/10.1016/j.foodhyd.2013.07.012

Silva, A. C. Q., Silvestre, A. J. D., Vilela, C., & Freire, C. S. R. (2022). Natural Polymers-Based Materials: A Contribution to a Greener Future. *Molecules*, *27*(1). https://doi.org/10.3390/molecules27010094

Silva, N. H. C. S., Rodrigues, A. F., Almeida, I. F., Costa, P. C., Rosado, C., Neto, C. P., Silvestre, A. J. D., & Freire, C. S. R. (2014). Bacterial cellulose membranes as transdermal delivery systems for diclofenac: in vitro dissolution and permeation studies. *Carbohydrate Polymers*, *106*, 264–269. https://doi.org/10.1016/j.carbpol.2014.02.014

Singhsa, P., Narain, R., & Manuspiya, H. (2018). Physical structure variations of bacterial cellulose produced by different Komagataeibacter xylinus strains and carbon sources in static and agitated conditions. *Cellulose*, *25*(3), 1571–1581. https://doi.org/10.1007/s10570-018-1699-1

Sliney, D. H. (2016). What is light? The visible spectrum and beyond. *Eye*, *30*(2), 222–229. https://doi.org/10.1038/eye.2015.252

Sørensen, B. E. (2013). A revised Michel?Lévy interference colour chart based on first?principles calculations. *European Journal of Mineralogy*, *25*(1), 5–10. https://doi.org/10.1127/0935?1221/2013/0025?2252

Souza, E. F., Furtado, M. R., Carvalho, C. W. P., Freitas-Silva, O., & Gottschalk, L. M. F. (2020). Production and characterization of Gluconacetobacter xylinus bacterial cellulose using cashew apple juice and soybean molasses. *International Journal of Biological Macromolecules*, *146*, 285–289. https://doi.org/https://doi.org/10.1016/j.ijbiomac.2019.12.180

Tagaya, A., & Koike, Y. (2001). Zero-birefringence polymers for optical devices. *Proc.SPIE*, *4594*, 348–358. https://doi.org/10.1117/12.446564

Tajima, K., Tahara, K., Ohba, J., Kusumoto, R., Kose, R., Kono, H., Matsushima, T., Fushimi, K., Isono, T., Yamamoto, T., & Satoh, T. (2020). Detailed Structural Analyses of Nanofibrillated Bacterial Cellulose and Its Application

as Binder Material for a Display Device. *Biomacromolecules*, *21*(2), 581–588. https://doi.org/10.1021/acs.biomac.9b01328

Tardy, B. L., Mattos, B. D., Otoni, C. G., Beaumont, M., Majoinen, J., Kämäräinen, T., & Rojas, O. J. (2021). Deconstruction and Reassembly of Renewable Polymers and Biocolloids into Next Generation Structured Materials. *Chemical Reviews*, *121*(22), 14088–14188. https://doi.org/10.1021/acs.chemrev.0c01333

Taylor, E. W., & Cramer, W. (1963). Birefringence of Protein Solutions and Biological Systems: II. Studies on TMV, Tropocollagen, and Paramyosin. *Biophysical Journal*, *3*(2), 143–154. https://doi.org/https://doi.org/10.1016/S0006-3495(63)86810-1

Thomas, B., Raj, M. C., B, A. K., H, R. M., Joy, J., Moores, A., Drisko, G. L., & Sanchez, C. (2018). Nanocellulose, a Versatile Green Platform: From Biosources to Materials and Their Applications. *Chemical Reviews*, *118*(24), 11575–11625. https://doi.org/10.1021/acs.chemrev.7b00627

Trovatti, E., Freire, C. S. R., Pinto, P. C., Almeida, I. F., Costa, P., Silvestre, A. J. D., Neto, C. P., & Rosado, C. (2012). Bacterial cellulose membranes applied in topical and transdermal delivery of lidocaine hydrochloride and ibuprofen: In vitro diffusion studies. *International Journal of Pharmaceutics*, *435*(1), 83–87. https://doi.org/https://doi.org/10.1016/j.ijpharm.2012.01.002

Ummartyotin, S., Juntaro, J., Sain, M., & Manuspiya, H. (2012). Development of transparent bacterial cellulose nanocomposite film as substrate for flexible organic light emitting diode (OLED) display. *Industrial Crops and Products*, *35*(1), 92–97. https://doi.org/https://doi.org/10.1016/j.indcrop.2011.06.025

van Aken, J. A., & Janeschitz-Kriegl, H. (1980). New apparatus for the simultaneous measurement of stresses and flow birefringence in biaxial extension of polymer melts. *Rheologica Acta*, *19*(6), 744–752. https://doi.org/10.1007/BF01521867

Wang, J., Tavakoli, J., & Tang, Y. (2019). Bacterial cellulose production, properties and applications with different culture methods – A review. *Carbohydrate Polymers*, *219*, 63–76. https://doi.org/https://doi.org/10.1016/j.carbpol.2019.05.008

Wang, S., Jiang, F., Xu, X., Kuang, Y., Fu, K., Hitz, E., & Hu, L. (2017). Super-Strong, Super-Stiff Macrofibers with Aligned, Long Bacterial Cellulose Nanofibers. *Advanced Materials*, *29*(35), 1702498. https://doi.org/https://doi.org/10.1002/adma.201702498

Wu, Z., Chen, S., Li, J., Wang, B., Jin, M., Liang, Q., Zhang, D., Han, Z., Deng, L., Qu, X., & Wang, H. (2023). Insights into Hierarchical Structure–Property–Application Relationships of Advanced Bacterial Cellulose Materials. *Advanced Functional Materials*, *n/a*(n/a), 2214327. https://doi.org/https://doi.org/10.1002/adfm.202214327

Yamada, Y., Yukphan, P., Vu, H. T. L., Muramatsu, Y., Ochaikul, D., & Nakagawa, Y. (2012). Subdivision of the genus Gluconacetobacter Yamada, Hoshino and Ishikawa 1998: the proposal of Komagatabacter gen. nov., for strains accommodated to the Gluconacetobacter xylinus group in the α-Proteobacteria. *Annals of Microbiology*, *62*(2), 849–859. https://doi.org/10.1007/s13213-011-0288-4

Yamanaka, S., Watanabe, K., Kitamura, N., Iguchi, M., Mitsuhashi, S., Nishi, Y., & Uryu, M. (1989). The structure and mechanical properties of sheets prepared from bacterial cellulose. *Journal of Materials Science*, *24*(9), 3141–3145. https://doi.org/10.1007/BF01139032

Yang, J., Du, M., Wang, L., Li, S., Wang, G., Yang, X., Zhang, L., Fang, Y., Zheng, W., Yang, G., & Jiang, X. (2018). Bacterial Cellulose as a Supersoft Neural Interfacing Substrate. *ACS Applied Materials & Interfaces*, *10*(39), 33049–33059. https://doi.org/10.1021/acsami.8b12083

Yu, W., Xiang, N., Li, M., Shen, G., Zhou, X., Huang, Z., Zhang, Y., Zhou, H., & Li, D. (2021). Prediction of birefringence for polymer optical products based on a novel molecular chain orientation model. *Polymer*, *233*, 124230. https://doi.org/https://doi.org/10.1016/j.polymer.2021.124230

Yuan, X., & Cheng, G. (2015). From cellulose fibrils to single chains: understanding cellulose dissolution in ionic liquids. *Physical Chemistry Chemical Physics*, *17*(47), 31592–31607. https://doi.org/10.1039/C5CP05744B

Zeng, M., Laromaine, A., & Roig, A. (2014). Bacterial cellulose films: influence of bacterial strain and drying route on film properties. *Cellulose*, *21*(6), 4455–4469. https://doi.org/10.1007/s10570-014-0408-y

Zhang, C., Cao, J., Zhao, S., Luo, H., Yang, Z., Gama, M., Zhang, Q., Su, D., & Wan, Y. (2020). Biocompatibility evaluation of bacterial cellulose as a scaffold material for tissue-engineered corneal stroma. *Cellulose*, *27*(5), 2775–2784. https://doi.org/10.1007/s10570-020-02979-0

Zhang, W., Wang, X., Li, X., Zhang, L., & Jiang, F. (2020). A 3D porous microsphere with multistage structure and component based on bacterial cellulose and collagen for bone tissue engineering. *Carbohydrate Polymers*, *236*, 116043. https://doi.org/https://doi.org/10.1016/j.carbpol.2020.116043

Zhao, X., Chen, S., Wu, Z., Sheng, N., Zhang, M., Liang, Q., Han, Z., & Wang, H. (2022). Toward continuous high-performance bacterial cellulose macrofibers by implementing grading-stretching in spinning. *Carbohydrate Polymers*, *282*, 119133. https://doi.org/https://doi.org/10.1016/j.carbpol.2022.119133

Zhou, Y., Starkey, J., & Mansinha, L. (2004). Identification of Mineral Grains in a Petrographic Thin Section Using Phi- and Max-Images. *Mathematical Geology*, *36*(7), 781–801. https://doi.org/10.1023/B:MATG.0000041179.79093.87